Published OnlineFirst June 24, 2021; DOI: 10.1158/1078-0432.CCR-21-0714

RASAL2 Confers Collateral MEK/EGFR Dependency in Chemoresistant Triple-Negative Breast Cancer

Siang-Boon Koh[1,2], Kenneth Ross[1,2,3], Steven J. Isakoff[1,2], Nsan Melkonjan[1], Lei He[1,2], Karina J. Matissek[1,2], Andrew Schultz[1], Erica L. Mayer[2,4], Tiffany A. Traina[5], Lisa A. Carey[6], Hope S. Rugo[7], Minetta C. Liu[8], Vered Stearns[9], Adam Langenbucher[1,2], Srinivas Vinod Saladi[1,2], Sridhar Ramaswamy[1,2,3,10], Michael S. Lawrence[1,2,3], and Leif W. Ellisen[1,2,10]

ABSTRACT

Purpose: While chemotherapy remains the standard treatment for triple-negative breast cancer (TNBC), identifying and managing chemoresistant tumors has proven elusive. We sought to discover hallmarks and therapeutically actionable features of refractory TNBC through molecular analysis of primary chemoresistant TNBC specimens.

Experimental Design: We performed transcriptional profiling of tumors from a phase II clinical trial of platinum chemotherapy for advanced TNBC (TBCRC-009), revealing a gene expression signature that identified *de novo* chemorefractory tumors. We then employed pharmacogenomic data mining, proteomic and other molecular studies to define the therapeutic vulnerabilities of these tumors.

Results: We reveal the RAS-GTPase-activating protein (RAS-GAP) RASAL2 as an upregulated factor that mediates chemotherapy resistance but also an exquisite collateral sensitivity to combination MAP kinase kinase (MEK1/2) and EGFR inhibitors in TNBC. Mechanistically, RASAL2 GAP activity is required to confer kinase inhibitor sensitivity, as RASAL2-high TNBCs sustain basal RAS activity through suppression of negative feedback regulators SPRY1/2, together with EGFR upregulation. Consequently, RASAL2 expression results in failed feedback compensation upon co-inhibition of MEK1/2 and EGFR that induces synergistic apoptosis *in vitro* and *in vivo*. In patients with TNBC, high RASAL2 levels predict clinical chemotherapy response and long-term outcomes, and are associated via direct transcriptional regulation with activated oncogenic Yes-Associated Protein (YAP). Accordingly, chemorefractory patient-derived TNBC models exhibit YAP activation, high RASAL2 expression, and tumor regression in response to MEK/EGFR inhibitor combinations despite well-tolerated intermittent dosing.

Conclusions: These findings identify RASAL2 as a mediator of TNBC chemoresistance that rewires MAPK feedback and cross-talk to confer profound collateral sensitivity to combination MEK1/2 and EGFR inhibitors.

Introduction

Triple-negative breast cancer (TNBC), defined by a lack of estrogen and progesterone receptor expression and HER2 amplification, remains a poor prognosis breast cancer subset. Most TNBCs share common molecular and histologic features including frequent *TP53* mutation, high proliferative index, and expression of a basal-like gene expression signature upon hierarchical clustering analysis. However, TNBC is a heterogeneous disease, representing multiple clinically and biologically distinct subgroups that remain to be fully defined (1). Furthermore, TNBC is associated with a paucity of actionable genetic alterations. Consequently, the primary systemic treatment modality for this disease remains cytotoxic chemotherapy (2).

Interest in platinum-based chemotherapy for TNBC was prompted by preclinical data suggesting that platinum may be more effective for breast tumors harboring *BRCA1* mutations, the majority of which are TNBC. We and others subsequently carried out clinical trials demonstrating higher response rates for *BRCA1/2*-mutant compared with nonmutant TNBC (3, 4). Nonetheless, even in the setting of *BRCA1/2* mutations only approximately half of patients with metastatic TNBC experience a clinically significant treatment response. As with other standard chemotherapy agents, responses occur in less than 30% of patients without such mutations. Patients whose tumors continue to progress despite chemotherapy are characterized by a particularly aggressive course and short survival.

Outside of *BRCA1/2*-mutant TNBC, which responds not only to platinum but also to recently FDA-approved PARP inhibitors, the promise of rational therapeutic targeting for TNBC has been elusive. Emerging application of immunotherapy such as immune checkpoint inhibitors appears promising, but the benefits may be restricted to only a subset of patients (5). The most prevalent somatic oncogene mutation in TNBC involves the PI3K catalytic subunit gene *PIK3CA* (~10% of tumors), and inactivating mutations in the PI3K inhibitory phosphatase gene *PTEN* are equally common (6). Despite some early promising results, it remains to be determined how effective PI3K-targeted therapy will be in metastatic TNBC, and whether *PIK3CA* and

[1]Massachusetts General Hospital Cancer Center, Boston, Massachusetts. [2]Harvard Medical School, Boston, Massachusetts. [3]Broad Institute of MIT and Harvard University, Cambridge, Massachusetts. [4]Dana-Farber Cancer Institute, Boston, Massachusetts. [5]Memorial Sloan Kettering Cancer Center, New York, New York. [6]University of North Carolina at Chapel Hill, Chapel Hill, North Carolina. [7]University of California San Francisco, San Francisco, California. [8]Georgetown Lombardi Comprehensive Cancer Center, Washington, District of Columbia. [9]Johns Hopkins University and Sidney Kimmel Cancer Center, Baltimore, Maryland. [10]Ludwig Center at Harvard, Harvard University, Boston, Massachusetts.

Note: Supplementary data for this article are available at Clinical Cancer Research Online (http://clincancerres.aacrjournals.org/).

Current address for S.V. Saladi: Department of Otolaryngology, Head and Neck Surgery, Massachusetts Eye and Ear Infirmary, Boston, Massachusetts; Broad Institute of MIT and Harvard, Cambridge, Massachusetts.

Corresponding Author: Leif W. Ellisen, Massachusetts General Cancer Center, Massachusetts General Hospital, Boston, MA 02114. Phone: 617 429-1659; E-mail: lellisen@mgh.harvard.edu

Clin Cancer Res 2021;27:4883–97

doi: 10.1158/1078-0432.CCR-21-0714

Published OnlineFirst June 24, 2021; DOI: 10.1158/1078-0432.CCR-21-0714

Translational Relevance

Chemotherapy remains the mainstay of treatment for most triple-negative breast cancers (TNBC). Unfortunately, there are currently no clinically used biomarkers that distinguish sensitive from resistant tumors, and no established alternative therapeutic options for chemorefractory cases. Here we show that high-level RASAL2 is a mediator of a TNBC subset that is refractory to standard chemotherapy, resulting in poor outcomes for these patients. However, RASAL2 RAS-GTPase-activating protein activity in these tumors leads to altered RAS signaling homeostasis and dependence on EGFR upregulation, resulting in a selective sensitivity to combination MEK1/2 and EGFR inhibition. Despite limited success of this therapeutic combination in other settings, the potent apoptotic responses observed even with low and intermittent inhibitor dosing suggests the potential clinical utility of the combination selectively for RASAL2-high TNBC.

PTEN alterations will prove to be useful predictors. Even more poorly understood is deregulation of the MAPK pathway in this disease. Gene expression profiling has suggested that activation of this pathway may be particularly prevalent in TNBC (7). The mechanisms involved are unclear, as mutations in canonical MAPK activators such as *RAS* and *RAF* are rare in these tumors. Alternative means of MAPK activation have been proposed in a subset of tumors, including truncating mutations in the *NF1* gene, and deregulation of microRNAs and the dual specific phosphatase DUSP4 (8). Unfortunately, traditional assessments of pathway activity in TNBC have not been successful in predicting clinical responses to relevant targeted inhibitors (9), highlighting a central unmet need in the field. MAPK deregulation in TNBC is likely to be complex, potentially due to the numerous feedback mechanisms whose contribution *in vivo* has not been well established (10). Furthermore, the relation of MAPK status to treatment response with standard chemotherapy remains a provocative but underexplored area.

We previously reported results of a multi-center phase II clinical trial of cisplatin or carboplatin for first- or second-line treatment of patients with metastatic TNBC, TBCRC009 (4). Here, we employed molecular analysis of tumor specimens from TBCRC009 as a starting point to identify rational potential treatment options for the most patients with chemorefractory TNBC. Transcriptome analysis reveals a gene signature that defines this platinum resistance, but surprisingly also predicts collateral sensitivity to inhibition of MEK1/2 and EGFR pathways. We find that a key driver of these phenotypes is RASAL2, a RAS-GTPase-activating protein (RAS-GAP) reported to have context-dependent pro- and anti-tumorigenic roles in different cancers (11). As no prior work had linked RASAL2 to either chemotherapy response or specific therapeutic vulnerabilities in cancer, we sought to understand the clinical contribution and mechanism of RASAL2 in TNBC.

Materials and Methods

Patient sample collection and analyses

Formalin-fixed paraffin-embedded primary tumors from patients with metastatic TNBC were collected from the multicenter phase II clinical trial TBCRC009. Each patient in the trial provided written informed consent, and the study was approved by the Institutional Review Boards at each participating site (4). Total RNA from the tumors was hybridized onto Affymetrix HuGene1v1 microarrays. Raw expression values in the form of CEL files were processed and normalized using RMA in the R Bioconductor package. The highly refractory tumor (HRT) signature was discovered following a *t* test on platinum-sensitive versus platinum-resistant samples as follows: inconsistent and unexpressed probe sets on the Affymetrix HuGene1v1 microarrays were first filtered by thresholding all values to a minimum value (8), then a minimum fold change (1.5) and minimum range (25) across all the samples. The *P* values from the *t*-test signature were corrected for multiple hypothesis testing with a Benjamini–Hochberg correction method. The HRT signature corresponds to 121 probe sets with FDR < 0.25, mapping to 129 genes (Supplementary Table S1). Tumor response/resistance was evaluated locally using CT according to RECIST 1.0 every two cycles for the first four cycles and every three cycles thereafter. *De novo* platinum-resistant (HRT) samples were defined by the established clinical criteria as sum of longest tumor diameter increase >20%. The HRT signature metagene was generated using the weighted average of $\log_2$ expression of the probe sets, with low metagene scores being associated with *de novo* progression in TBCRC009. Probe sets were mapped to gene symbols and other microarray platforms using the R Bioconductor package biomaRt.

Drug-sensitivity data derived from validated cancer cell lines treated with a broad range of therapeutic compounds was downloaded from the Wellcome Sanger/MGH Genomics of Drug Sensitivity in Cancer website (12). The HRT metagene was calculated as described above for the cell lines covered by the RMA expression data except that probe sets in the HRT signature was mapped to Ensembl gene IDs using the R Bioconductor package biomaRt. Pearson correlations and *P* values were calculated between the HRT meta-gene and drug sensitivity in R using the cor.test method.

Cell lines and chemicals

All cell lines (MDA-MB-157, MDA-MB-468, MDA-MB-231, HCC38, HCC1937, HS578T) were obtained from the Massachusetts General Hospital Center for Molecular Therapeutics bank and subjected to high-density SNP genotyping to confirm their identity. Cells were grown in RPMI medium (Lonza) supplemented with 10% FBS (Sigma) as well as 1% penicillin/streptomycin (Gibco), and were used up to a maximum of 20 passages following thawing. Cell lines were tested negative for *Mycoplasma* using MycoAlert Mycoplasma Detection Kit (Lonza). Cisplatin resistance state cells were generated using a previously reported protocol (13). Cisplatin (Enzo Life Sciences) was dissolved in 0.9% sodium chloride; PD0325901 (Selleck Chemicals) and gefitinib (Selleck Chemicals) were dissolved in DMSO.

Cell viability and clonogenic assays

Cells were seeded 24 hours before treatment exposure for specified duration. For short-term cell viability assays, cells were seeded in 96-well plates (1,500–2,500 cells/well) and treated for 72 hours. Cell viability was measured by CellTiter-Glo Luminescent Assay (Promega) according to manufacturer's instructions. For long-term clonogenic assay, cells were seeded in 6- or 12-well plates (3,000–5,000 cells/well) and treated for a defined period before being released into fresh medium for 1–2 weeks. Cells were fixed with 70% methanol and stained with 0.1% crystal violet. Crystal violet was solubilized using 10% acetic acid and the absorbance was measured at 590 nm.

Immunoblotting, immunostaining, and reverse-phase protein array screen

For immunoblotting, cells (MDA-MB-468, HCC1937, HCC38) were seeded in 6-well plates at 250,000–500,000 cells per well and, following indicated treatment exposure, were lysed in RIPA buffer

Published OnlineFirst June 24, 2021; DOI: 10.1158/1078-0432.CCR-21-0714

(50 mmol/L Tris pH 8, 150 mmol/L sodium chloride, 5 mmol/L EDTA, 0.5% sodium deoxycholate, 0.1% sodium dodecyl sulfate, 1% NP-40, protease and phosphatase inhibitors). Protein concentrations were quantified by the Bio-Rad Protein Assay (Bio-Rad). Equal amounts of protein were resolved using the SDS-PAGE system and transferred to polyvinylidene difluoride membranes (Millipore). Membranes were blocked with 3% BSA and incubated with primary antibodies overnight followed by horseradish peroxidase (HRP)-conjugated secondary antibodies for 1 hour. The signal was detected by enhanced chemiluminescence solution (PerkinElmer). For immunostaining, cells were seeded in 8-well chamber slides (ibidi) at 2,000–5,000 cells per well and, following treatment exposure, were fixed with 4% paraformaldehyde, stained with appropriate antibodies and counterstained with DAPI. The full list of antibodies and related details are in Supplementary Tables S2 and S3. For reverse-phase protein array (RPPA) screens, isogenic MDA-MB-468 cells were lysed in RPPA lysis buffer (1% Triton X-100, 50 mmol/L HEPES, pH 7.4, 150 mmol/L sodium chloride, 1.5 mmol/L magnesium chloride, 1 mmol/L EGTA, 100 mmol/L sodium floride, 10 mmol/L sodium pyrophosphate, 1 mmol/L sodium orthovanadate, 10% glycerol, protease and phosphatase inhibitors). The screens were conducted as previously described at MD Anderson Cancer Center RPPA Facility (14). Briefly, cell lysates were 2-fold serial diluted for 5 dilutions (from undiluted to 1:16 dilution) and arrayed on nitrocellulose-coated slide in 11 × 11 format. Samples were probed with antibodies and visualized by 3,3′-diaminobenzidine colorimetric reaction. Relative protein levels for each sample were determined by interpolation of each dilution curves from the standard curve. All the data points were normalized for protein loading and transformed to linear values, which can be used for comparative purposes. Full details are at: https://www.mdanderson.org/research/research-resources/core-facilities/functional-proteomics-rppa-core/rppa-process.html.

Chromatin immunoprecipitation

Cells were subjected to cross-linking by addition of 1% formaldehyde for 10 minutes at room temperature, followed by addition of 125 mmol/L glycine to stop the reaction. Cell pellet was then lysed in RIPA buffer (10 nmol/L Tris pH 7.5, 150 mmol/L sodium chloride, 1 mmol/L EDTA, 1% sodium deoxycholate, 0.1% sodium dodecyl sulfate, 1% NP-40, protease inhibitor) for 2 hours at 4°C. Lysate was sonicated for five times, each time 7.5 minutes. Sonicated chromatin was precleared with Protein G Sepharose bead (GE Healthcare) preblocked with BSA and sonicated salmon sperm DNA. Samples were incubated with antibodies overnight and with beads for another 2 hours, both at 4°C. Beads were washed with wash buffer I (150 mmol/L sodium chloride, 20 mmol/L Tris pH 8.1, 2 mmol/L EDTA, 0.1% sodium dodecyl sulfate, 1% Triton-X-100), wash buffer II (150 mmol/L sodium chloride, 20 mmol/L Tris pH 8.1, 2 mmol/L EDTA, 0.02% sodium dodecyl sulfate, 1% Triton-X-100), wash buffer III (250 mmol/L lithium chloride, 10 mmol/L Tris pH 8.1, 1 mmol/L EDTA, 1% sodium deoxycholate, 1% NP-40), and Tris-EDTA buffer (10 mmol/L Tris pH 7.9, 1 mmol/L EDTA). After these washes, beads were incubated for 3 hours at 55°C, followed by overnight incubation at 65°C, in elution buffer (10 mmol/L Tris pH 7.9, 1 mmol/L EDTA, 0.5% sodium dodecyl sulfate, 10 μg RNase A, 10 μg proteinase K). DNA was purified with Qiaquick PCR purification kit (Qiagen). qPCR was performed with iQ SYBR Green Supermix reagent (Bio-Rad), using primers of RASAL2 at peak 1 (TGCTGTCATGTCCAGTCTGC; CTGAAGGCCAAGCCTCAAAC) and Peak 2 (ACACTCAAGGC-CAGTTTGTCT; GCTCA-GTCACTAAGAACCTGTGT).

Lentiviral transduction

HEK293T cells were transfected while at 70% confluency in 10-cm dishes with pLenti CMV Puro DEST (w118-1; Addgene #17452; ref. 15) or R777-E235 Hs.RASAL2 (Addgene #70519) together with lentiviral packaging plasmids using the CalPhos Mammalian Transfection Kit (Clontech Laboratories). Plasmids of RASAL2 wild-type and GAP point mutant K417E were gifts from Karen Cichowski (16). Conditioned medium containing lentiviral particles were collected 18 hours after transfection and were filtered with 0.45-μmol/L pore filter (Millipore). Filtered media were then used to transduce target cells (MDA-MB-468, HCC1937, HCC38), with addition of polybrene (Sigma) at a final concentration of 10 μg/mL to increase infection efficiency (which was 70%–90%). The transduced cells were selected using 1 μg/μL puromycin (Sigma) for a week and were maintained in medium with 1 μg/μL puromycin.

Cytotoxicity agent combination assay and synergy calculation

Cells (MDA-MB-468, HCC1937, HCC38) were seeded in 96-well plates (1,500–2,500 cells/well) for 24 hours in 96-well plates and then treated with a serial dilution of each agent in a 6 × 6 concentration format that included single-agent concentrations for 96 hours. Cell viability was measured by CellTiter-Glo Luminescent Assay (Promega) according to manufacturer's instructions. To quantify synergy, readout from the cytotoxicity assays was analyzed on the basis of the Bliss independence, Loewe or highest single agent models, as described previously (17–19).

Animal studies

All animals were housed and treated in accordance with protocols approved by the Subcommittee on Research Animal Care at the Massachusetts General Hospital (Boston, MA). Subcutaneous xenografts of MDA-MB-468 cells were conceived by implanting 2×10^6 cells in 50% Matrigel/50% PBS in the flanks of female 6 to 10 weeks old athymic nu/nu mice. Patient-derived xenograft (PDX) TM01278 mouse model was procured from The Jackson Laboratory. Data on tumor response to cisplatin were obtained from The Jackson Laboratory (20). PD0325901 (Selleck Chemicals) and gefitinib (Selleck Chemicals) were given by oral gavage at 20 and 75 mg/kg, respectively. These agents were given, singly or in combination, on days 1, 3, 5, 8, and 11 of the treatment period. This dosing regimen was less intensive than that employed in prior studies, where PD0325901 was typically used at 20–50 mg/kg daily or on alternating days, and gefitinib at 100 mg/kg daily (21–25). Tumor size was measured twice weekly using vernier caliper based on the formula $\pi/6 \times \text{width} \times \text{width} \times \text{length}$.

Ex vivo generation

Tumor specimens for patient-derived *ex vivo* cultures were collected under the IRB protocol 93-085 with written informed consent from chemoresistant patients on the day of surgery. They were then digested mechanically and enzymatically using human tumor dissociation kit (Miltenyi Biotec). Cultures were initially grown in EpiCult medium (STEMCELL Technologies) with 10% FBS. Once the cultures began to establish, serum-free medium was used to discourage proliferation of fibroblasts. During passaging, fibroblasts were further separated from the samples using trypsin-EDTA. To assess efficacy of drugs, the cultures were seeded in 8-well chamber slides (ibidi) at 70% confluency and exposed to 72-hour drug treatment. Cell viability was assessed using trypan blue. Immunostaining of these cultures was also performed, as described above.

Published OnlineFirst June 24, 2021; DOI: 10.1158/1078-0432.CCR-21-0714

Databases

In silico analysis was conducted using data sourced from the Genomics of Drug Sensitivity in Cancer (GDSC; ref. 12), cBioPortal for Cancer Genomics (26, 27), and Gene expression-based Outcome for Breast cancer Online (GOBO; ref. 28; Supplementary Table S4). GDSC was used to obtain drug sensitivity data as well as associated gene expression in cell lines. cBioPortal and GOBO were used to obtain transcriptomic data as well as associated clinical outcomes.

Statistical analyses

Data were analyzed using the GraphPad Prism built-in tests. Figures were generated using GraphPad Prism or Microsoft Excel. Unless otherwise denoted, comparison between two groups was performed using Student *t* test, unpaired or paired. Comparison among three or more groups were performed using either one-way or two-way (if with time factor) ANOVA test, followed by *post hoc* Tukey multiple comparisons test. Correlation between two datasets was performed using Pearson or Spearman correlation coefficient. The following asterisk rating system for *P* value was used: *, $P < 0.05$; **, $P < 0.01$; ***, $P < 0.001$; ****, $P < 0.0001$.

Results

A unique gene signature marks platinum resistance and predicts collateral MAPK pathway vulnerability in TNBC

We focused on the population of patients enrolled in TBCRC009 who experienced *de novo* disease progression in response to platinum, clinically defined by RECIST as a greater than 20% increase tumor size at the initial on-treatment assessment compared with pre-treatment baseline (4). We performed gene expression profiling of pre-treatment tumor specimens from 55 patients, 7 of whom experienced *de novo* progression (**Fig. 1A** and **B**). Treatment-related clinical factors did not account for the poor response of these tumors (Supplementary Fig. S1A), nor did established molecular markers of TNBC: these tumors included basal and nonbasal TNBC, as well as both *TP53* and *PIK3CA* mutant and wild-type tumors (Supplementary Fig. S1B). In contrast, supervised hierarchical clustering revealed a 129-gene signature corresponding to genes that were predominantly downregulated in these seven highly refractory tumors, which we termed the HRT signature (**Fig. 1B**; Supplementary Fig. S1C, see Materials and Methods). Supporting its association with aggressive TNBC, in an independent cohort of patients with breast cancer who experienced metastatic relapse the HRT signature predicted a shorter time to metastasis among patients with TNBC but not patients with non-TNBC (**Fig. 1C**; ref. 29). Multiple prognosis-associated signatures have been reported for breast cancer, and several of these signatures in fact identify a common group of tumors (30). Thus, we asked whether the HRT signature corresponded to any other gene expression signatures reported to distinguish breast cancer subtypes (31–34). None of the established signatures we tested overlapped with the HRT signature, and none identified the 7 patients with HRT (**Fig. 1D**). Collectively, these findings suggest that the HRT signature marks a unique phenotype associated with platinum resistance and poor outcomes in advanced TNBC.

To investigate potential functional associations of the HRT phenotype, we next examined a large-scale pharmacogenomic database derived from validated human cancer cell lines treated with a broad range of therapeutic compounds (12). Among the 252 therapeutic agents tested in more than 800 cell lines, the compounds whose sensitivity was most highly correlated with HRT targeted the MEK/ERK pathway (**Fig. 1E**). In line with this finding, the top 25 compound hits also included multiple inhibitors that target the upstream receptor tyrosine kinase (RTK) EGFR (**Fig. 1F**). In each case, low HRT scores (as observed in tumors of *de novo* progressing patients in TBCRC009) were associated with high sensitivity to MEK1/2 inhibitors (MEKi; Supplementary Fig. S1D). We independently confirmed this association by conducting dose–response analyses of TNBC cell lines with varying HRT scores treated with MEKi (**Fig. 1G**).

To delineate the underlying basis for this association, we asked whether expression of the HRT signature might predict MEKi sensitivity independent of established genomic predictors. Indeed, while mutations in *KRAS, HRAS, NRAS*, and *BRAF* genes were associated with increased sensitivity to all five tested MEKis as anticipated (Supplementary Fig. S1E), the HRT score was not statistically associated with these mutations (Supplementary Fig. S1F). Thus, the HRT phenotype is a determinant of MEKi sensitivity distinct from *RAS/RAF* mutations. Collectively, these data suggest that the HRT phenotype is associated with a poor response to platinum chemotherapy but denotes a potential therapeutic vulnerability to MEK inhibition.

The HRT gene RASAL2 confers MEKi sensitivity via deregulation of dynamic feedback signaling

To unveil direct mechanisms of MEKi sensitivity predicted by the HRT signature, we next assessed the correlation of each of the genes with this sensitivity in the pharmacogenomic database. The single upregulated HRT signature gene, encoding the RAS-GAP RASAL2, was among the most highly associated with MEKi sensitivity across all cell lines (**Fig. 2A**; Supplementary Fig. S2A). Furthermore, RASAL2 was the most highly correlated with sensitivity among all HRT genes in independent testing of TNBC lines (Supplementary Fig. S2B). We also generated an isogenic, cell-based platinum resistance model of TNBC using a previously established protocol (13). Notably, the resulting platinum resistant state was associated with MEKi sensitivity, and with upregulation of RASAL2 in these cells (**Fig. 2B**; Supplementary Fig. S2C). Critically, we found that RASAL2 expression itself was sufficient to induce both platinum resistance and MEKi sensitivity in TNBC cells (**Fig. 2C**). Long-term clonogenic assays further corroborated sensitivity to MEK inhibition conferred by RASAL2 expression (**Fig. 2D**).

To elucidate the mechanism of MEKi sensitivity conferred by RASAL2, we first asked whether the GAP activity of RASAL2 was required for this effect. Compared with wild-type RASAL2, expression of a well-established GAP-deficient RASAL2 mutant had little or no effect on MEKi sensitivity (**Fig. 2E**; Supplementary Fig. S2D; ref. 16), demonstrating the requirement for RASAL2 GAP activity. This finding was provocative given that MEKi sensitivity is typically linked to activation rather than inhibition of RAS/RAF signaling (35). Thus, we examined the effects of RASAL2 expression on canonical readouts of RAS activity via the MAPK and PI3K signaling pathways in TNBC cells. Surprisingly, despite the contribution of GAP activity in this context, RASAL2 expression did not induce noticeable changes in baseline (steady-state) ERK1/2 and AKT phosphorylation in TNBC cells (**Fig. 2F** and **G**). Consistent with these data, there was no correlation between RASAL2 protein expression and the steady-state levels of phosphorylated ERK1/2 in primary breast tumors (Supplementary Fig. S2E).

We hypothesized that this observation might be explained by feedback adaptations that would maintain RAS output in the face of high RASAL2 levels (7, 36). Among the molecular players implicated in such feedback mechanisms are SPRY1 and SPRY2, which are typically induced in response to ERK/MAPK activation to mediate negative feedback control of RAS activity (37). Indeed, wild-type but

Published OnlineFirst June 24, 2021; DOI: 10.1158/1078-0432.CCR-21-0714

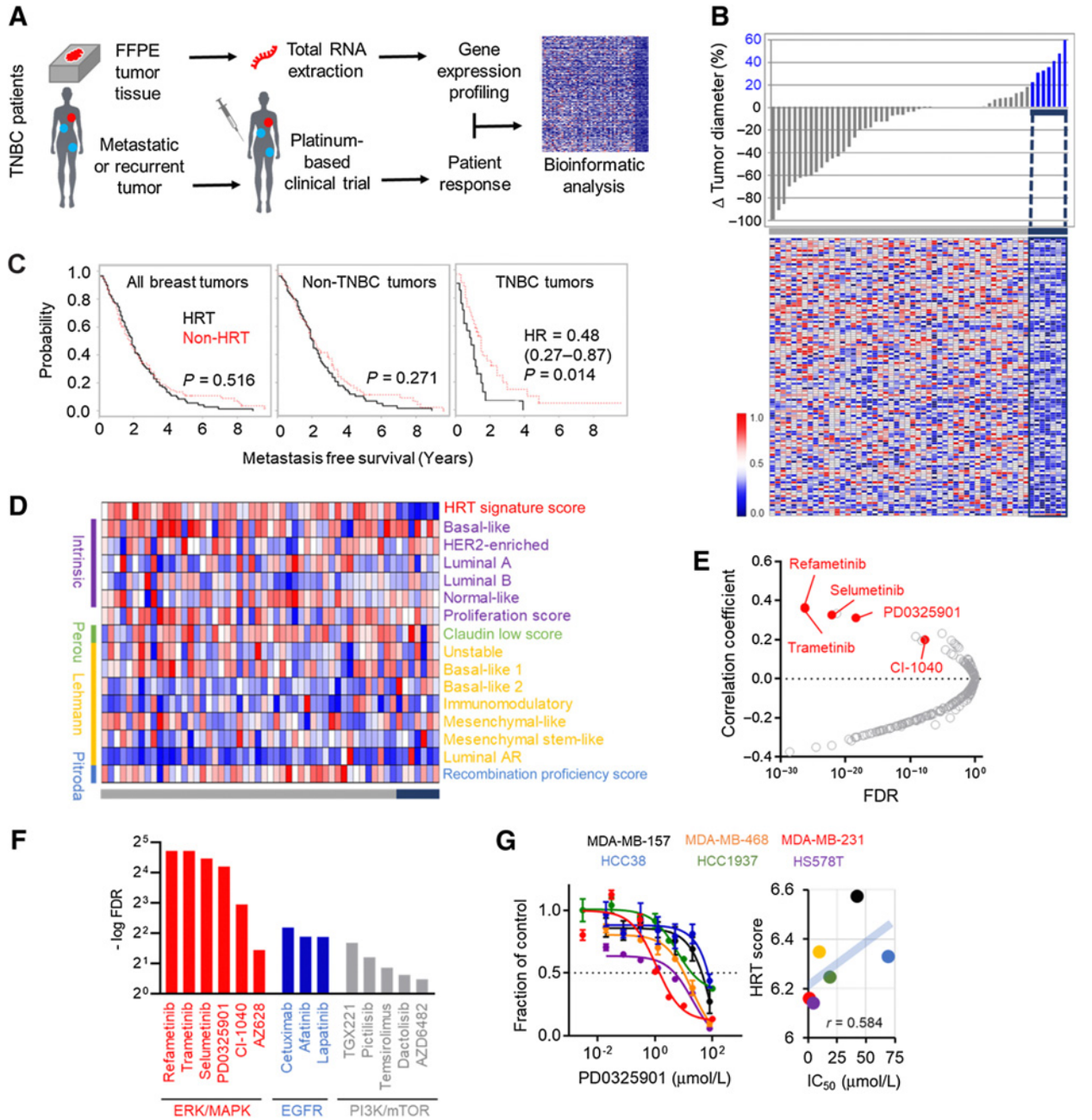

Figure 1.

A unique gene expression signature predicts collateral sensitivity to MEK1/2 inhibition in platinum-resistant TNBC. **A,** Overview of TNBC tumor collection, processing, and analyses from the phase II clinical trial TBCRC009. **B,** Waterfall plot (top) of post-treatment change in tumor diameter (best response). Each bar denotes 1 patient ($n = 55$). Seven patients experienced clinically defined *de novo* disease progression (blue bars). Heatmap below shows expression of the 129 genes (rows) comprising the HRT signature in the corresponding tumors. **C,** Kaplan–Meier analyses of metastasis-free survival in the EMC-192 cohort of patients with advanced breast cancer, stratified by the HRT metagene expression (Bos and colleagues, 2009). Log-rank test was performed. **D,** Heatmap representing metagene scores of each indicated breast cancer signature (rows) among the 55 profiled tumors (columns) in TBCRC009. HRTs are shown at far right. **E,** Scatter plot summarizing pharmacogenomic screen results from 252 drugs and drug candidates in more than 800 cell lines (Garnett and colleagues, 2012). The *y*-axis correlation coefficient reflects the relationship between IC_{50} and HRT metagene among human tumor cell lines. *X*-axis indicates FDR. Five top drugs whose sensitivity was most highly correlated with the HRT signature are highlighted (red dots). **F,** Top three pathways targeted by drugs whose sensitivity was correlated with HRT. These drugs were among the top 25 whose sensitivity was most correlated with HRT. Each bar represents an inhibitor of the indicated pathway. **G,** Relationship between IC_{50} for MEKi PD0325901 (left, dose–response curves following 72-hour treatment) and HRT metagene (graph at right) in the indicated TNBC cell lines (MDA-MB-157, MDA-MB-468, MDA-MB-231, HCC38, HCC1937, HS578T). Data are represented as mean ± SD, $n = 3$ independent experiments. Pearson *r* is shown. See also Supplementary Fig. S1.

Published OnlineFirst June 24, 2021; DOI: 10.1158/1078-0432.CCR-21-0714

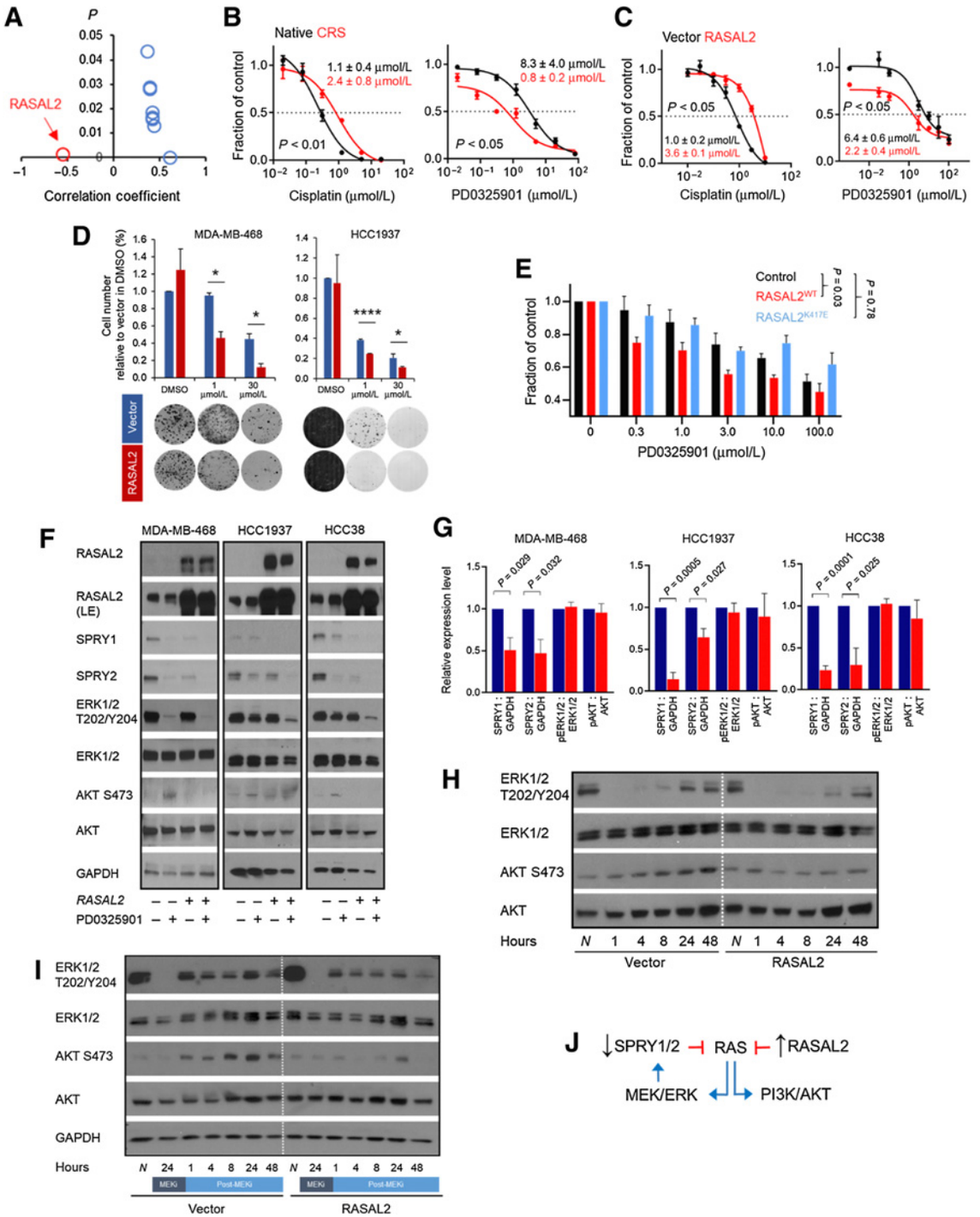

Figure 2.

RASAL2 disrupts dynamic feedback signaling to confer MEK inhibitor sensitivity. **A,** RASAL2 is the single upregulated HRT signature gene that is highly associated with MEKi (trametinib) sensitivity in breast cancer cell lines. Circles depict 10 genes showing statistically significant association with trametinib sensitivity in breast cancer cell lines, including RASAL2. Pearson correlation coefficient was performed. **B,** Isogenic platinum-resistant TNBC cells acquire MEKi sensitivity. Native and cisplatin resistance state (CRS) MDA-MB-468 cells were treated with cisplatin or MEKi PD0325901 for 72 hours. Data are represented as mean ± SD, $n = 3$ independent experiments. *P* values by paired *t* test. **C,** RASAL2 expression confers both cisplatin resistance and MEKi sensitivity in TNBC cells. Vector control and RASAL2-overexpressing MDA-MB-468 cells were treated with cisplatin or MEKi PD0325901 for 72 hours. Data are represented as mean ± SD, $n = 3$ independent experiments. *P* values by paired *t* test. **D,** RASAL2 expression induces MEKi sensitivity. Clonogenic assays of vector control and RASAL2-overexpressing TNBC cells treated with MEKi PD0325901 for 5 days before being released into fresh medium over 2 weeks. (*Continued on the following page.*)

Published OnlineFirst June 24, 2021; DOI: 10.1158/1078-0432.CCR-21-0714

not GAP-deficient RASAL2 expression was sufficient to reduce basal SPRY1/2 levels in TNBC cells (**Fig. 2F** and **G**; Supplementary Fig. S2D). Furthermore, high RASAL2 expression was significantly associated with low SPRY1/2 levels in primary TNBC tumors (Supplementary Fig. S2F). The effect of RASAL2 on steady-state SPRY1/2 levels was consistently observed in multiple tested TNBC models, and as noted was associated with preserved baseline AKT and ERK1/2 phosphorylation (**Fig. 2F** and **G**). These findings suggest that increased RASAL2 expression is accompanied by decreased SPRY1/2 levels that may contribute to preserved steady-state RAS output in TNBC.

Attenuated SPRY1/2 expression in the setting of RASAL2 expression suggested to us a mechanism by which this altered feedback to RAS could contribute to RASAL2-associated MEKi sensitivity. Specifically, MEK inhibition would normally be expected to downregulate SPRY1/2 as a feedback response to attenuated ERK1/2 activity, resulting in relief of negative feedback to RAS that would ultimately induce rebound PI3K and MAPK survival signaling (38, 39). However, in RASAL2-overexpressing cells, the already low levels of SPRY1/2 could limit the ability of further SPRY1/2 downregulation to induce this rebound. Consistent with this hypothesis, in control cells SPRY1/2 expression indeed decreased concomitant with ERK1/2 T202/Y204 dephosphorylation and rebound AKT S473 phosphorylation 24 hours after MEKi (**Fig. 2F**). In contrast, in RASAL2-overexpressing cells, the already low baseline levels of SPRY1/2 were associated with substantially attenuated AKT rebound phosphorylation after MEKi (**Fig. 2F**). Levels of phosphorylated ERK1/2 were also consistently lower in RASAL2-expressing cells post MEKi (**Fig. 2F**). To explore this model in more detail, we performed time-course studies following MEK inhibition. These experiments confirmed attenuated rebound AKT phosphorylation and prolonged suppression of ERK1/2 phosphorylation between 24 and 48 hours after MEKi treatment in RASAL2-overexpressing cells (**Fig. 2H**). Orthogonal experiments involving washout of MEKi demonstrated diminished rebound activation of both AKT and ERK1/2 phosphorylation in RASAL2-expressing cells following washout, as anticipated previously (**Fig. 2I**). Taken together, these findings implicate RASAL2 in a disrupted equilibrium of RAS negative regulators at steady state, resulting in an enfeebled feedback loop to RAS and PI3K following MEKi treatment that could otherwise contribute to survival signaling in TNBC cells (**Fig. 2J**).

MEKi plus EGFRi synergistically inhibit RASAL2-expressing TNBC

Other than MEK1/2, the top target predicted for selective inhibitor sensitivity by the HRT signature was EGFR (**Fig. 1F**). We hypothesized that this observation might point to EGFR signaling as an additional mechanism required to sustain downstream signaling despite high RASAL2 levels in primary TNBC. As such, inhibition of EGFR might represent an additional therapeutic vulnerability specifically in the RASAL2-high context. Consistent with this hypothesis, we found a strong positive correlation between expression of RASAL2 and EGFR, but not other RTKs, in both TNBC cell lines and primary tumors (**Fig. 3A**; Supplementary Fig. S3A and S3B; refs. 26, 40, 41). Copy-number gains of *RASAL2* and *EGFR* are also statistically associated in TNBC (Supplementary Fig. S3C). Furthermore, similar to MEK inhibition, we found that rebound phosphorylation of AKT and ERK1/2 was attenuated following EGFR inhibition in RASAL2-expressing TNBC, both during drug incubation and following drug washout (**Fig. 3B**). Collectively, these data suggest a selective pressure for EGFR expression and an associated EGFR dependency in RASAL2-expressing TNBC. We therefore wished to know whether drug combinations involving both MEKi and EGFR inhibitor (EGFRi) could represent a potent and specific approach for these chemorefractory tumors.

To test the potential efficacy of combination therapy in this context, we exposed isogenic TNBC lines with or without RASAL2 overexpression to MEKi+EGFRi combinations. We observed significantly enhanced growth inhibition with the combination following RASAL2 expression in TNBC lines (Supplementary Fig. S3D). To formally determine whether this inhibition was synergistic, we performed integrative analyses involving drug synergy predictions and systematic combination cytotoxicity assays that captured a matrix of concentration ratios (**Fig. 3C**; ref. 18). Reproducibly, independent computational models of synergy (Loewe, Bliss, highest single agent) demonstrated selective and synergistic growth inhibition with combination therapy in RASAL2-expressing cells compared with vector in multiple TNBC models even at low concentrations (**Fig. 3C** and **D**). This synergy was accompanied by heightened levels of apoptosis, as evidenced by cleaved caspase 3 (**Fig. 3E**). Next, to evaluate the efficacy and synergy of this combination *in vivo* while minimizing potential toxicity, we employed xenograft models to test doses and treatment frequencies that were lower than those typically employed with these compounds in mice (see Materials and Methods; refs. 21–25). As anticipated, single-agent MEKi and EGFRi did not induce significant growth suppression in control TNBC xenografts, although EGFRi alone did attenuate growth of RASAL2-expressing tumors to some extent (**Fig. 3F**). In contrast, the combination of these agents delayed tumor growth without overt host toxicities (Supplementary Fig. S3E), and most notably induced rapid, significant regression associated with strong cleaved caspase 3 positivity exclusively in RASAL2-expressing tumors (**Fig. 3G** and **H**; Supplementary Fig. S3F). Collectively, both *in vitro* and *in vivo* data support the notion that RASAL2 expression in TNBC confers a synergistic therapeutic vulnerability

(*Continued.*) Data are represented as mean ± SD, $n = 3$ independent experiments. *P* values by two-tailed *t* test, *, $P < 0.05$; ****, $P < 0.0001$. **E,** MEKi sensitivity is dependent on RAS GAP activity. Vector control, RASAL2 wild-type and RASAL2 K417E GAP point mutant MDA-MB-468 cells were treated with MEKi PD0325901 for 72 hours. Data are represented as mean ± SEM, $n = 3$ independent experiments. *P* values by one-way ANOVA test, followed by Tukey test. **F,** Immunoblots of vector control and RASAL2-overexpressing TNBC cells. RASAL2 deregulates SPRY1/2 expression and AKT/ERK1/2 phosphorylation post MEKi. Cells were treated with either DMSO or 25 nmol/L MEKi PD0325901 for 24 hours. LE denotes long exposure. Representative images from three independent experiments are shown. **G,** Quantification of densitometry values of denoted baseline protein expression in vector (blue) versus RASAL2-expressing (red) TNBC cells (MDA-MB-468, HCC1937, HCC38). Data are represented as mean ± SEM, $n = 3$ independent experiments. *P* values by two-tailed *t* test. **H,** Time course of vector control and RASAL2-overexpressing MDA-MB-468 treated with 25 nmol/L MEKi PD0325901. Rebound phosphorylation of ERK1/2 and AKT is attenuated following RASAL2 expression. N denotes DMSO control. Representative images from two independent experiments are shown. **I,** Immunoblots showing RASAL2-induced deregulation of rebound phosphorylation following MEKi washout. Vector control and RASAL2-overexpressing TNBC cells were treated with 100 nmol/L MEKi PD0325901 (24 hours) before being released into fresh medium. N denotes DMSO control. Representative images from two independent experiments are shown. **J,** Model of deregulated RAS homeostasis in the presence of high RASAL2. High RASAL2 expression is offset by low SPRY1/2 expression to maintain RAS output. Reduced basal levels of SPRY1/2 impairs the compensatory feedback to RAS normally mediated via SPRY1/2 downregulation following MEK1/2 inhibition, thereby sensitizing RASAL2-high cells to this inhibition. See also Supplementary Fig. S2.

Published OnlineFirst June 24, 2021; DOI: 10.1158/1078-0432.CCR-21-0714

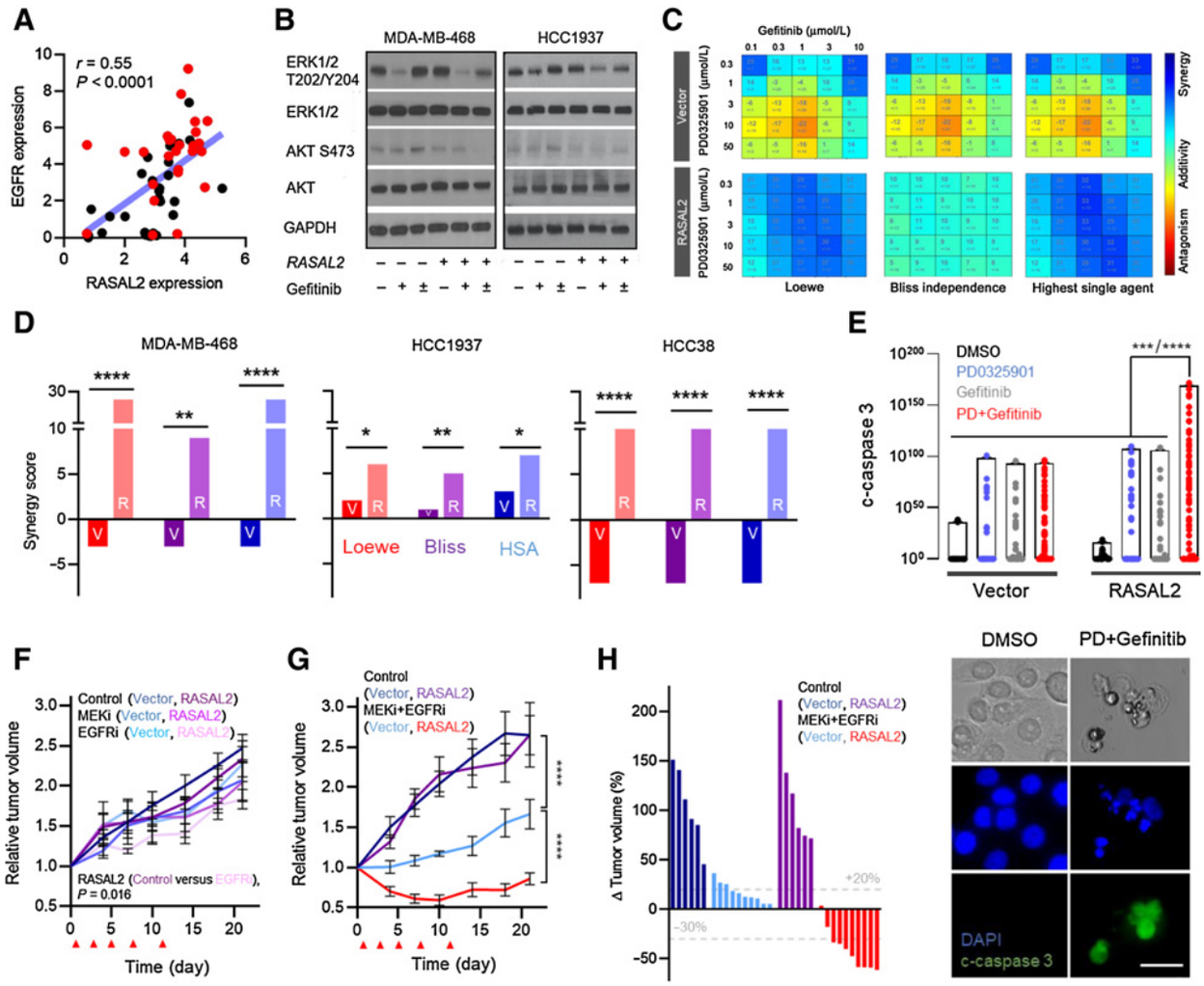

Figure 3.

Dual inhibition of MEK1/2 and EGFR selectively and synergistically inhibits RASAL2-expressing TNBC. **A,** RASAL2 expression is correlated with EGFR expression in human breast tumor lines (Ghandi and colleagues, 2019). Each dot represents one cell line, with red dots denoting TNBC lines. Pearson *r* and *P* value are shown. **B,** Immunoblots showing RASAL2-induced deregulation of rebound phosphorylation of ERK1/2 and AKT following EGFRi washout. Vector control and RASAL2-overexpressing TNBC cells were treated with 100 nmol/L EGFRi gefitinib for 24 hours (+) before being released into fresh medium for 2 hours (±). Representative images from two independent experiments are shown. **C,** MEKi (PD0325901) and EGFRi (gefitinib) selectively and synergistically inhibit RASAL2-overexpressing MDA-MB-468 cells. Cells were exposed to increasing concentrations of gefitinib (*x*-axis) and PD0325901 (*y*-axis) for 96 hours. Loewe, Bliss, and highest single agent synergy models were used to define drug–drug interactions across the dose ratio surface (Koh and colleagues, 2018). The higher the score is (blue), the more synergistic that dose ratio is. Two independent experiments were performed. **D,** Quantification of median synergy scores derived from dose ratio surface in TNBC cell lines. Isogenic cell lines were treated as described in **C**. V denotes vector cells; R denotes RASAL2 cells. In each case, two independent experiments were performed. *P* values by two-tailed *t* test, *, $P < 0.05$; **, $P < 0.01$; ****, $P < 0.0001$. **E,** Quantitative immunofluorescence showing greater cell death in RASAL2-expressing TNBC cells treated with MEKi+EGFRi. MDA-MB-468 cells were exposed to the indicated drugs for 96 hours. Top, each dot shows the relative cleaved-caspase 3 level per cell. More than 100 cells were analyzed per condition. Data are represented as mean ± SEM. *P* value by one-way ANOVA test, followed by Tukey test, ***, $P < 0.001$; ****, $P < 0.0001$. Representative photomicrographs are shown below. Scale bar, 50 μm. **F,** MDA-MB-468 xenograft assay showing that single-agent treatment using MEKi (PD0325901) or EGFRi (gefitinib) minimally inhibits tumor growth *in vivo*. Arrowheads denote treatment days (1, 3, 5, 8, 11). Vector $n = 5$, RASAL2 $n = 5$ in all treatment arms. **G,** Combined MEKi (PD0325901) and EGFRi (gefitinib) induces significant tumor regression in RASAL2-expressing xenografts. Arrowheads denote treatment days as in **F**. Control $n = 6$, combination $n = 10$ in both genotypes. *P* value by two-way ANOVA test, followed by Tukey test ****, $P < 0.0001$. **H,** Percentage change in volume of individual tumors in each arm shown in **G**. See also Supplementary Fig. S3.

to the combination of MEKi+EGFRi in chemoresistant TNBC even despite nonintensive dosing.

RASAL2 mediates chemoresistance in TNBC

Given the association of RASAL2 expression with platinum resistance in the TBCRC009 cohort, we wished to test the contribution of RASAL2 to clinical chemoresistance in TNBC. RASAL2 expression in TNBC cells was sufficient to confer resistance to multiple clinically used chemotherapeutic agents including cisplatin, doxorubicin, and gemcitabine (**Fig. 4A**). To test the impact of RASAL2 expression on clinical chemoresistance, we first analyzed outcomes of patients with TNBC from the largest global

Published OnlineFirst June 24, 2021; DOI: 10.1158/1078-0432.CCR-21-0714

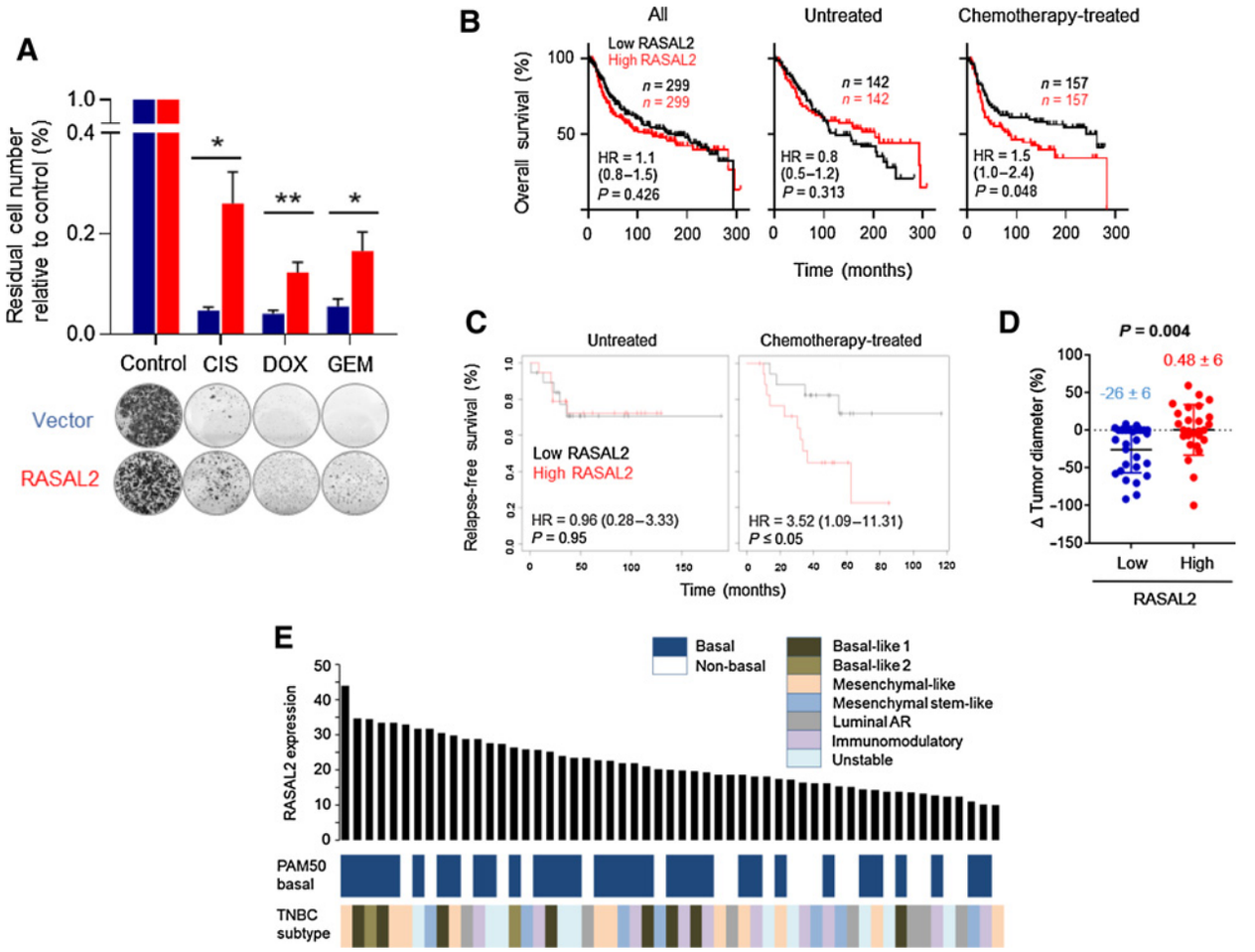

Figure 4.

RASAL2 predicts poor response to chemotherapy in patients with TNBC. **A,** RASAL2 expression induces chemoresistance. Clonogenic assays of vector control and RASAL2-overexpressing MDA-MB-468 cells treated with either 1 μmol/L cisplatin (CIS), 50 nmol/L doxorubicin (DOX), or 30 nmol/L gemcitabine (GEM) for 24 hours before being released into drug-free medium for 1 week. Representative images of cell colonies are shown below. Data are represented as mean ± SEM, $n = 3$ independent experiments. P values by two-tailed t test, *, $P < 0.05$; **, $P < 0.01$. **B,** Kaplan–Meier analyses of overall survival of patients with TNBC in METABRIC (Curtis and colleagues, 2012; Pereira and colleagues, 2016). Patients with TNBC were stratified by median of RASAL2 expression according to whether they had been chemotherapy-treated. Log-rank test was performed. **C,** Kaplan–Meier analyses of relapse-free survival in multiple independent cohorts of patients with TNBC (Gyorffy and colleagues, 2010). Patients with TNBC were stratified by tertiles of RASAL2 expression according to whether they had been chemotherapy-treated (untreated, $n = 19$ in each arm; treated, $n = 17$ in low RASAL2 and 18 in high RASAL2). Log-rank test was performed. **D,** Tumor diameter change (best response) in TBCRC009 patients following platinum treatment, grouped by median expression of RASAL2. Each dot represents 1 patient. Values > 20% are clinically defined as *de novo* progression. Data are represented as mean ± SD. P values by two-tailed t test, with mean ± SEM indicated. **E,** Distribution of RASAL2 expression in breast tumors from TBCRC009, by TNBC subtype (Lehmann and colleagues, 2011). Each black bar represents one patient. See also Supplementary Fig. S4.

breast cancer cohort, METABRIC (Molecular Taxonomy of Breast Cancer International Consortium; refs. 42, 43). In particular, we sought to distinguish a chemopredictive effect of RASAL2 from a strictly prognostic effect, as a prior study had reported generally poor outcomes in patients with RASAL2-high TNBC but did not explore the therapeutic context (44). Accordingly, we analyzed outcomes based on RASAL2 expression, comparing chemotherapy-treated versus chemotherapy-untreated patients with TNBC. While RASAL2 was not prognostic in untreated patients with TNBC, it was significantly associated with poor outcomes selectively in chemotherapy-treated patients with TNBC (**Fig. 4B**; Supplementary Fig. S4A). These findings were recapitulated in independent patient cohorts, as RASAL2 was again predictive of outcomes in treated but not untreated patients with TNBC (**Fig. 4C**; ref. 28). Furthermore, RASAL2 was associated with in-breast treatment response to chemotherapy in primary TNBC. Specifically, we found that tumors of patients who did not achieve a pathologic complete response (pCR) to preoperative therapy, a strong prognostic indicator, expressed higher levels of RASAL2 compared with those who achieved pCR (Supplementary Fig. S4B and S4C).

We further investigated the clinical association of RASAL2 with chemotherapy response in TNBC by examining tumor regression as a function of median RASAL2 expression in the TBCRC009 cohort (**Fig. 1A**). As predicted, patients whose tumors expressed high RASAL2 levels experienced a significantly poorer response to platinum

Published OnlineFirst June 24, 2021; DOI: 10.1158/1078-0432.CCR-21-0714

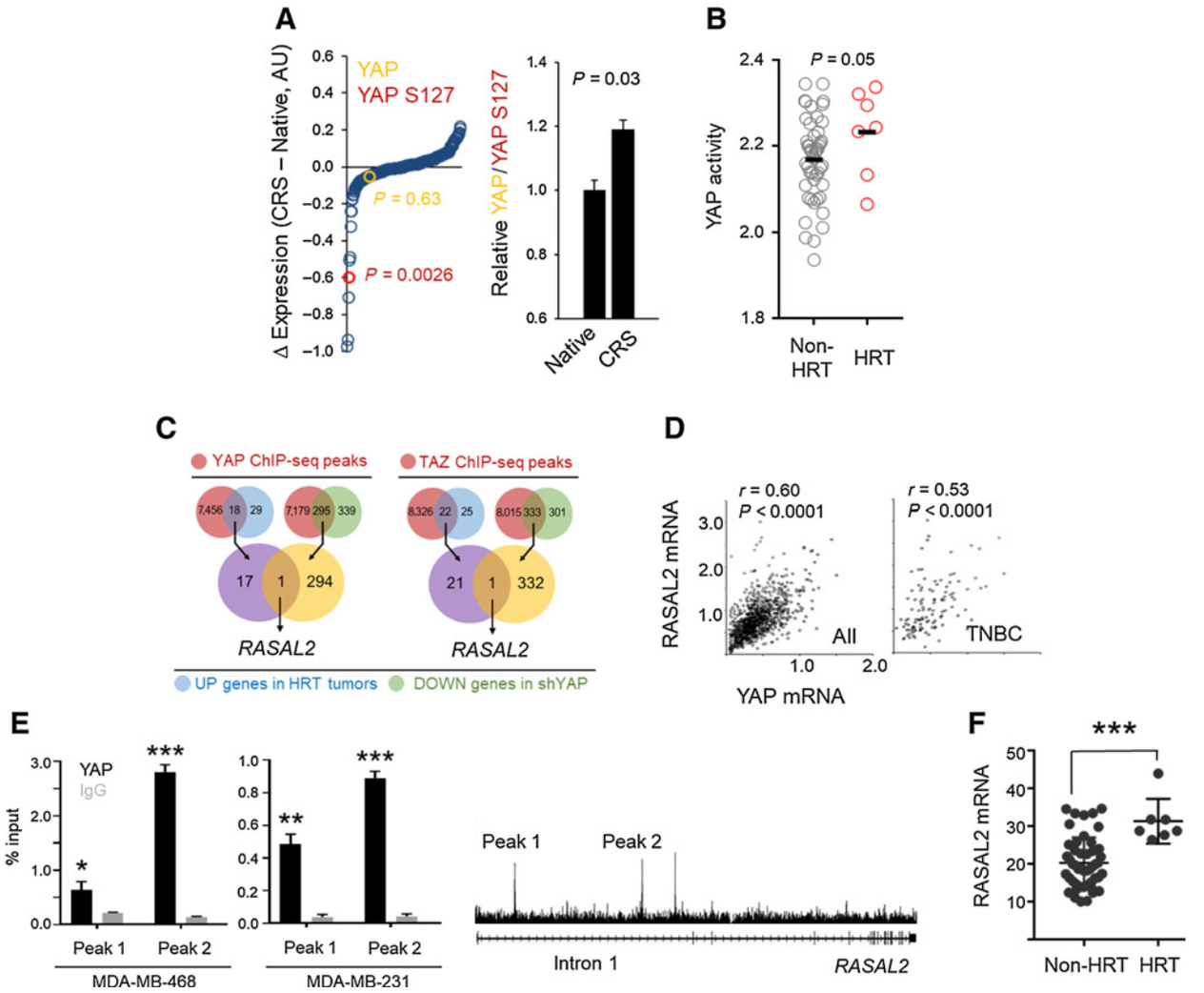

Figure 5.

RASAL2 is a direct YAP/TAZ transcriptional target in TNBC. **A,** RPPA screen of native and CRS MDA-MB-468 cells. Changes in 217 (phospho)proteins were plotted (*y*-axis, AU = arbitrary unit). Bar graph at right shows the level of active YAP (YAP/YAP S127) in the isogenic pair. Data are represented as mean ± SD. *P* values by two-tailed *t* test. **B,** YAP activity is increased in HRTs in TBCRC009. YAP activity is defined by a gene expression signature derived from lentiviral knockdown of endogenous YAP in MDA-MB-468 cells (Supplementary Fig. S5C). *P* value by unpaired *t* test. **C,** Convergent analysis of YAP/TAZ ChIP-seq (Zanconato and colleagues, 2016), and HRT and YAP knockdown transcriptomes. Number in circles denotes genes associated with YAP (left) or TAZ (right) ChIP-seq peaks (red circles) that were upregulated in the HRTs ($P < 0.025$, blue circles) or downregulated following shYAP knockdown in MDA-MB-468 cells (FDR < 0.25, fold change > 1.2, green circles). Overlapping genes between HRT and YAP knockdown analyses identified *RASAL2* as the single candidate YAP/TAZ-regulated gene in both settings. **D,** Correlation between YAP and RASAL2 expression in TCGA breast carcinoma (All) and TNBC samples (Gao and colleagues, 2013). Pearson *r* and *P* value are shown. **E,** ChIP analysis confirms direct binding of YAP to the *RASAL2* locus in TNBC cells. Bar graphs reflect YAP binding to the respective peaks shown in the YAP ChIP-seq trace from MDA-MB-231 (Zanconato and colleagues, 2016). Data are represented as mean ± SD, $n = 3$ independent experiments. *P* values by two-tailed *t* test, *, $P < 0.05$; **, $P < 0.01$; ***, $P < 0.001$. **F,** *RASAL2* is significantly elevated in the HRT versus non-HRT in TBCRC009. Data are represented as mean ± SD. *P* value by two-tailed *t* test, ***, $P < 0.001$. *RASAL2* is the most significantly upregulated gene between HRT and non-HRT (Supplementary Fig. S5F). See also Supplementary Fig. S5.

treatment than those with low RASAL2 (**Fig. 4D**). In fact, all tumors that exhibited low (less than median) RASAL2 expression were initially stable or regressed in response to platinum, while all tumors that had progressed at first assessment showed greater than median expression (**Fig. 4D**). We also found that RASAL2 expression was independent of established TNBC subtypes defined by gene expression signatures (**Fig. 4E**). Taken together, our data suggest that RASAL2 confers a chemoresistant phenotype, resulting in poor long-term outcomes in TNBC across recognized TNBC subtypes.

RASAL2 is a direct YAP transcriptional target in chemorefractory TNBC

We next sought to uncover potential regulatory mechanisms for RASAL2 in TNBC, initially through analysis of the isogenic platinum resistance model (**Fig. 2B**). We thus performed proteomic analysis of the matched platinum-sensitive and platinum-resistant TNBC cells using a validated RPPA (14). This analysis revealed significant alterations in the Hippo/Yes-Associated Protein (YAP) pathway between the platinum-resistant and platinum-sensitive

Published OnlineFirst June 24, 2021; DOI: 10.1158/1078-0432.CCR-21-0714

states. These alterations included decreased expression of the positive Hippo regulator Merlin/NF2 (Supplementary Fig. S5A) and associated activation of YAP, an established oncogenic transcriptional cofactor and chemoresistance driver that is negatively regulated by Hippo signaling (**Fig. 5A**; Supplementary Fig. S5A and S5B; refs. 45, 46). Correspondingly, we also uncovered evidence that YAP activity is increased in chemoresistant/RASAL2-expressing TNBC cases in TBCRC009, as analysis of a YAP gene expression signature derived from endogenous YAP knockdown in TNBC cells (Supplementary Fig. S5C) revealed an increase in YAP activity in platinum-refractory tumors compared with non-refractory tumors (**Fig. 5B**).

While the association of YAP with chemoresistance in several cancers including TNBC is well established, its downstream mediators remain largely unknown (47, 48). On the basis of the hypothesis that YAP may contribute to regulation of RASAL2 in this context, we then performed a convergent analysis that sought to reveal the subset of genes: (i) bound by YAP upon chromatin immunoprecipitation sequencing (ChIP-seq) in TNBC cells (49); (ii) regulated following endogenous YAP knockdown in TNBC (Supplementary Fig. S5C), and (iii) altered in tumors of the patients with HRT in TBCRC009 (**Fig. 5C**). This analysis revealed RASAL2 as the sole gene meeting these criteria, indicating that RASAL2 may be a direct YAP transcriptional target. RASAL2 was also identified in similar analyses incorporating ChIP-seq for the YAP-related co-factor TAZ in TNBC (**Fig. 5C**). Furthermore, RASAL2 was one of the HRT-associated genes both bound and regulated by YAP and TAZ in untransformed mammary epithelial cells (Supplementary Fig. S5D; refs. 50). These data collectively suggest RASAL2 may be an activated target of YAP in TNBC.

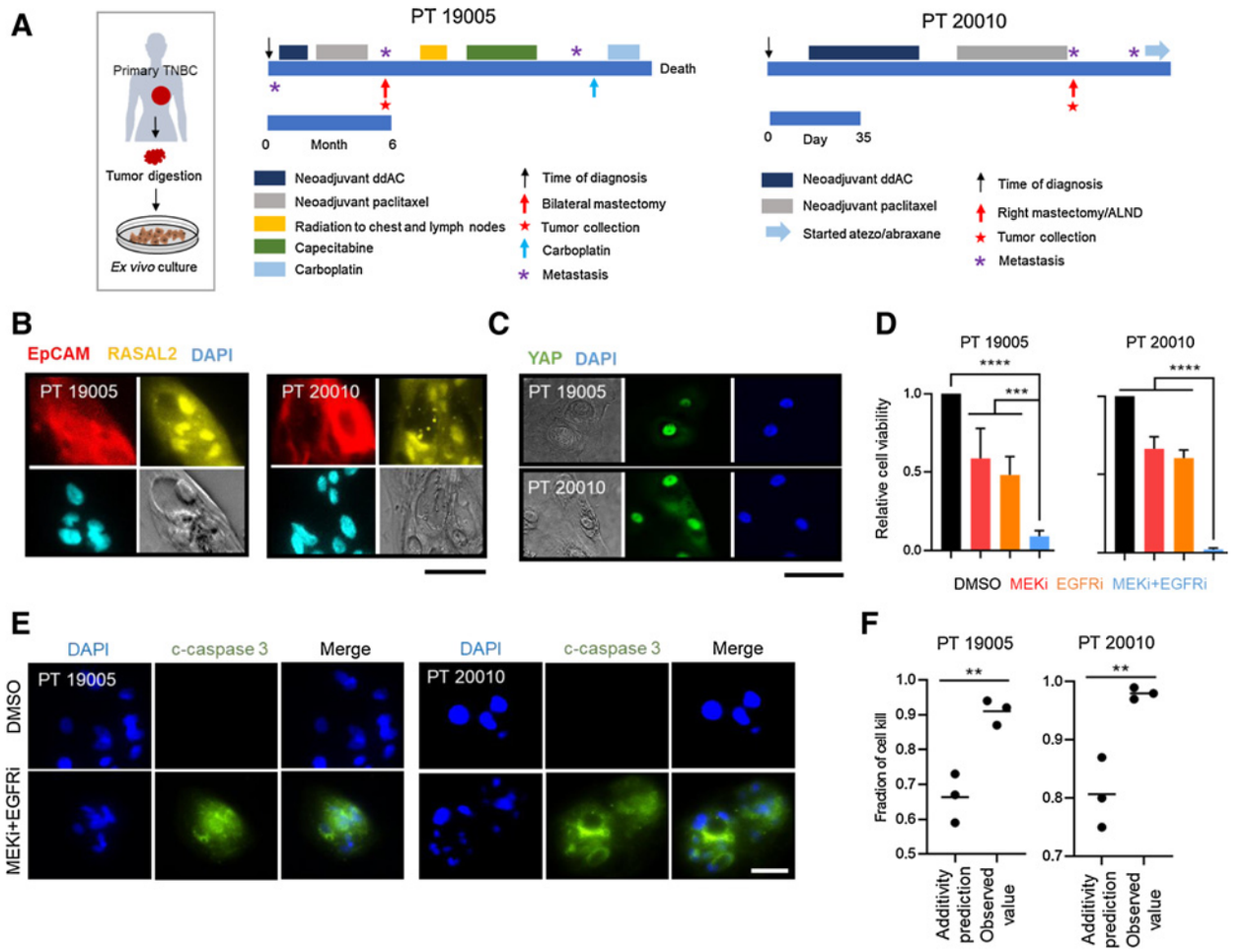

Figure 6.

Dual inhibition of MEK1/2 and EGFR is effective in chemorefractory patient-derived TNBC models. **A,** Patient timelines showing treatment modalities and sample collections. Red stars indicate tumor collection for *ex vivo* culture. ddAC, dose-dense adriamycin/cyclophosphamide; ALND, axillary lymph node dissection. Immunofluorescence showing EpCAM-positive tumor cells exhibit high RASAL 2 (**B**) and nuclear YAP (**C**) expression in primary cultures of TNBC specimens described in **A**. Scale bar, 50 μm. **D,** Cytotoxicity assays using patient-derived cultures. *Ex vivo* cultures were exposed to DMSO, MEKi PD0325901, EGFRi gefitinib, or the combination for 72 hours, and viable cells were counted 20 days later. Data are represented as mean ± SEM, $n = 3$ independent experiments. *P* values by two-tailed *t* test, ***, $P < 0.001$; ****, $P < 0.0001$. **E,** Immunofluorescence showing extensive cleaved caspase 3 in patient-derived cultures treated with MEKi+EGFRi combination for 24 hours. Scale bar, 50 μm. **F,** Synergy analysis of cell killing by MEKi+EGFRi. Bliss additivity (predicted) based on single-agent effects was compared with observed values of the combination in each case. Significant departure of fraction killed by the combination from the predicted values signifies drug synergy. *P* values by two-tailed *t* test, **, $P < 0.01$. See also Supplementary Fig. S6.

Published OnlineFirst June 24, 2021; DOI: 10.1158/1078-0432.CCR-21-0714

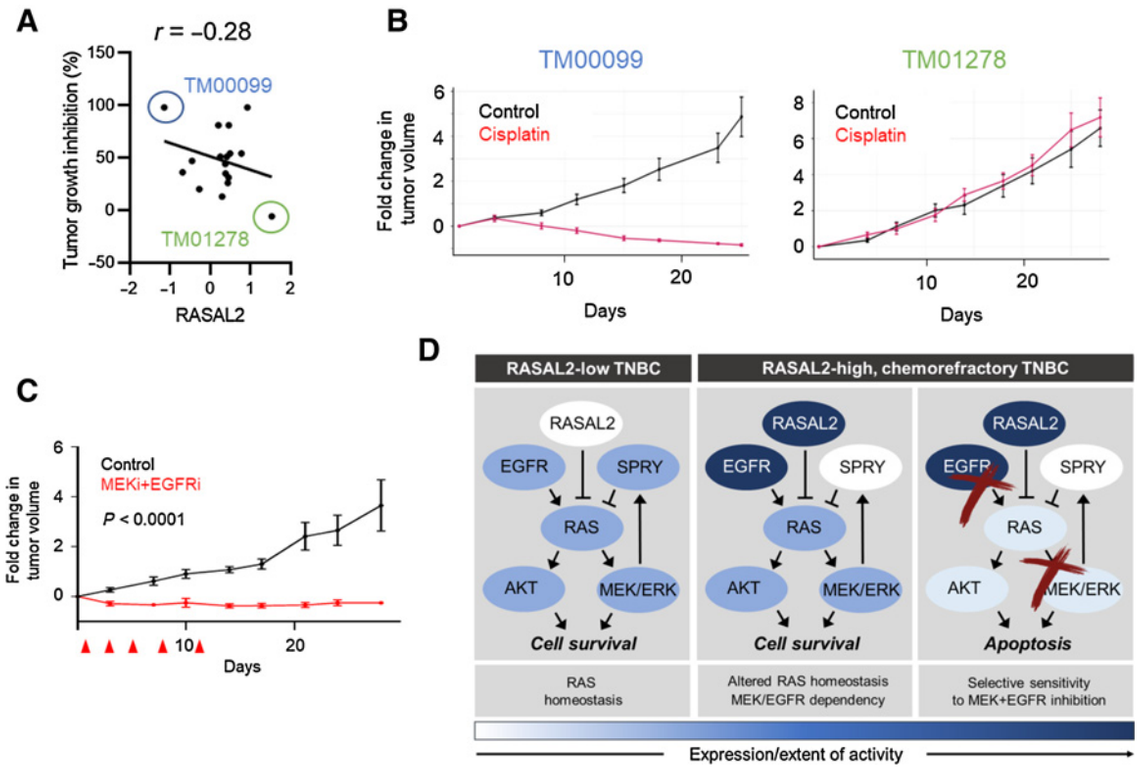

Figure 7.

RASAL2-high PDX tumors are chemoresistant but sensitive to dual inhibition of MEK1/2 and EGFR. **A,** RASAL2 expression is correlated with *in vivo* tumor response to cisplatin. Mice were treated with vehicle control or 2 mg/kg cisplatin (Krupke and colleagues, 2017). Each dot represents an independent TNBC PDX model. Tumor growth inhibition was defined as [1 − (mean volume of treated tumors)/(mean volume of control tumors)] × 100%. **B,** Fold change in tumor volume following cisplatin in two TNBC PDX models. Mice were treated as described in **A**, $n = 8$–10 per group. TM00099 tumors had the lowest RASAL2 expression, whereas TM01278 had the highest RASAL2 expression. **C,** Fold change in tumor volume following MEKi+EGFRi in RASAL2-high TM01278 PDX models. Mice were treated with vehicle control or PD0325901+gefitinib. Arrowheads denote treatment days (1, 3, 5, 8, 11). Control $n = 5$, combination $n = 5$. *P* value by two-way ANOVA test, followed by Tukey test. **D,** RAS homeostasis is achieved through the dynamic interplay among regulators including RASAL2, EGFR, and SPRY. In chemorefractory TNBC characterized by high RASAL2, a deregulated SPRY feedback loop and EGFR upregulation contribute to an altered state of RAS homeostasis (center), involving EGFR dependency and the inability to further suppress SPRY following MEK inhibition (right). These features render the RASAL2-expressing subset of TNBCs specifically vulnerable to the synergistic combination of MEK and EGFR inhibitors. See also Supplementary Fig. S7.

To further support these findings, we analyzed RNA-sequencing data from breast carcinomas in The Cancer Genome Atlas (TCGA). We found a strong positive correlation between RASAL2 and YAP expression among both TNBC cases and other breast cancer subtypes (**Fig. 5D**). Correspondingly, RASAL2 expression was correlated with YAP copy number in breast cancer (Supplementary Fig. S5E). We then performed direct ChIP analysis, which showed robust binding of YAP to the RASAL2 genomic locus in TNBC cell lines (**Fig. 5E**). Furthermore, RASAL2 was the topmost significantly elevated factor among the chemorefractory tumor subset in TBCRC009, where YAP was hyperactive (**Fig. 5B** and **F**; Supplementary Fig. S5F). Taken together, these findings suggest that YAP activation directly contributes to RASAL2 regulation in TNBC.

Synergistic sensitivity to MEKi plus EGFRi in chemorefractory patient-derived TNBC models

Our findings predict that patients' tumors exhibiting clinical resistance to chemotherapy will demonstrate YAP activation, high RASAL2 expression and high sensitivity to the MEKi+EGFRi combination. We tested this hypothesis by generating *ex vivo* cultures derived from TNBCs of patients who had failed to attain pCR following neoadjuvant chemotherapy (**Fig. 6A**; Supplementary Fig. S6A). As predicted, these models showed strong expression of nuclear (activated) YAP and endogenous RASAL2 (**Fig. 6B** and **C**; Supplementary Fig. S6B). Furthermore, compared with single-agent controls, MEKi+EGFRi induced dramatic cell killing in these cultures (**Fig. 6D**), including extensive apoptotic induction that was observed following brief exposure to the combination (**Fig. 6E**). Accordingly, synergy modeling based on additivity prediction showed that the enhanced inhibition was synergistic rather than additive (**Fig. 6F**). Thus, lethal chemorefractory tumors expressing high levels of RASAL2 are efficiently killed by the combination of MEKi+EGFRi.

RASAL2 predicts sensitivity to MEKi plus EGFRi in chemorefractory TNBC *in vivo*

Finally, we employed *in vivo* PDX models to test our specific hypothesis regarding the ability of RASAL2 to identify TNBC tumors that are at once highly refractory to chemotherapy but highly sensitive to combination MEKi plus EGFRi. We first examined the correlation between tumor-specific RASAL2 expression and *in vivo* platinum resistance in an established repository of TNBC PDX models (**Fig. 7A**; ref. 20). This analysis revealed that the most highly

platinum-responsive PDX model in the cohort exhibited the lowest RASAL2 expression, and conversely the most platinum-resistant model showed the highest RASAL2 level (**Fig. 7A** and **B**; ref. 20). Indeed, reminiscent of the HRTs in TBCRC009 trial (**Fig. 1A** and **B**), the refractory RASAL2-high tumor exhibited no response whatsoever to platinum chemotherapy compared with vehicle treatment (**Fig. 7B**). In dramatic contrast, this model exhibited a substantial response including tumor regression following MEKi plus EGFRi combination therapy, even employing an intermittent dosing schedule that was without overt host toxicity (**Fig. 7C**; Supplementary Fig. S7A and S7B). All together, these data suggest that RASAL2 expression underlies a subset of TNBC tumors characterized by little or no response to standard chemotherapy and poor overall survival. Yet the GAP-dependent rewiring of growth factor signaling engendered by RASAL2 results in an exquisite sensitivity of these tumors to combination therapy involving MEKi plus EGFRi (**Fig. 7D**).

Discussion

While chemotherapy still represents a potentially curative mainstay of systemic treatment for TNBC, little progress has been made in predicting which patients will or will not benefit from such treatment. To address this unmet need, we analyzed highly chemorefractory tumors from a phase II clinical trial of platinum chemotherapy for TNBC as a starting point to identify potential therapeutic vulnerabilities in this tumor subset (4). Through transcriptome profiling of patient tumors and human cell lines coupled with drug response studies in preclinical models, we discovered a unique gene expression signature of platinum-resistant TNBC that is notably associated with sensitivity to targeted inhibitors converging on the MAP kinase pathway. Our analysis revealed that a significant mediator of both of these phenotypes is upregulation of RASAL2, a RAS-GAP that is thought to have pleiotropic oncogenic and tumor suppressor functions in different cancer contexts (11). In TNBC, we demonstrate that RASAL2-expressing tumors maintain basal RAS activity through substantial rewiring of growth factor signaling, including attenuation of SPRY1/2-driven negative feedback and increased expression of EGFR. The associated cost of such adaptations to these otherwise aggressive tumors is an exquisite sensitivity to perturbation of these signaling pathways in the setting of combined MEK and EGFR inhibition. Thus, we observe a selective and synergistic susceptibility to MEKi+EGFRi combination in cell-based, xenograft, patient-derived *ex vivo* and patient-derived RASAL2-expressing TNBC models.

Prior work has implicated RASAL2 in various pathways mediating effects such as tumor growth and invasion, including in TNBC (11, 44). Here, we provide direct evidence that the poor outcomes associated with RASAL2 expression in TNBC are related to its ability to induce chemoresistance. Furthermore, our observation that YAP activation is associated with RASAL2 in chemorefractory TNBC provides new insights into prior studies demonstrating an association of YAP with chemoresistance and poor prognosis in basal-like breast cancer and TNBC (47, 51). The ability of RASAL2 expression to hallmark a distinct TNBC subset, at once refractory to conventional chemotherapy but potentially highly vulnerable to a targeted therapy combination, merits its further investigation as a potential clinical biomarker. In particular, recent work shows that phosphorylation of RASAL2 at S237 moiety promotes breast cancer progression independent of estrogen receptor status (52). Thus, posttranslational modifications of RASAL2 could be important determinants of its functions in breast and other cancers, and its role as a biomarker.

Sensitivity to MAPK inhibition in many cancers is typically associated with activation of this pathway, most notably through mutations in RAS and RAF family members (53). Thus, a remarkable finding of our study is that the (inhibitory) GAP activity of RASAL2 is required to mediate sensitivity to pathway inhibition, despite little effect of RASAL2 on steady-state ERK1/2 and AKT phosphorylation in TNBC *in vitro* or *in vivo*. We explain these observations in part by demonstrating that RASAL2 induces a concomitant reduction in the expression of the RAS negative regulators SPRY1/2. However, SPRY deregulation alone may be insufficient to sustain RAS signaling in RASAL2-expressing TNBC, and may be associated with distinct adaptations in different tumor mutational contexts (54). We observe strong dependency on EGFR signaling in RASAL2-high TNBC, as evidenced by a marked sensitivity to EGFR and EGFR/MEK inhibition. These findings all suggest an exquisite control of RAS/MAPK activity in RASAL2-expressing TNBC, mediated by multiple adaptive changes and with profound consequences for cell survival once the pathway is perturbed.

Multiple clinical trials employing combinations of MAPK and PI3K pathway inhibitors together with RTK inhibitors are currently underway for patients with TNBC. However, combining inhibitors of the RAS pathway without understanding the selective forces that lead to patient- and tumor-specific rewiring of this signaling has largely proven unsuccessful. For instance, a recent phase II trial evaluating MEKi and AKTi showed limited efficacy of this combination in patients with unselected advanced TNBC, although a small number of clinical responses were observed (9). In contrast, in PDX models of (rare) metaplastic TNBC harboring both PI3K/AKT/mTOR and RTK/MAPK alterations, MEKi- and PI3Ki-induced tumor regression, suggesting that targeting MEK and PI3K/AKT is a potentially viable strategy under specific contexts (55). In TNBC cell lines, co-targeting MEK1/2 and EGFR has been shown to induce synergistic growth inhibition and apoptosis, albeit to varying degrees (56). Our findings provide mechanistic insights and demonstrate that this strategy achieves selective synergism in the RASAL2 context.

The successful application of such targeted therapy combinations is often hampered by substantial toxicities. In humans, studies of MEKi PD0325901 have employed twice daily dosing and have observed significant adverse effects with prolonged treatment (57–59). Likewise, gefitinib is usually administered daily in humans, equivalent to the daily regimen typically employed in preclinical studies (60, 61). Our use of intermittent schedules of these inhibitors in mice achieved dramatic tumor regression in RASAL2-high tumors without overt toxicities, even with the combination regimen. These findings support the evaluation of alternative doses and schedules for such inhibitors and combinations in contexts where marked therapeutic vulnerabilities can be defined. Taken together, our findings support the clinical evaluation of MEKi+EGFRi combination selectively in the RASAL2-expressing subgroup of TNBC. More broadly, our study highlights the general importance of identifying and targeting unanticipated, collateral vulnerabilities in ostensibly refractory tumors as an effective approach for rational cancer therapy.

Authors' Disclosures

S.-B. Koh has a patent for RASAL2 biomarker pending. S.J. Isakoff reports grants from Translational Breast Cancer Research Consortium during the conduct of the study, as well as personal fees from Mylan, Myriad, OncoPep, Puma, Seattle Genetics, and Novartis; grants and personal fees from AbbVie; and grants from AstraZeneca and Merck outside the submitted work. E.L. Mayer reports other support from Lilly, Novartis, and Pfizer outside the submitted work. T.A. Traina reports other support from TBCRC during the conduct of the study, as well as grants, personal fees, and nonfinancial support from Roche, Astellas, Ayala, Daiichi Sankyo, and Gilead and

Published OnlineFirst June 24, 2021; DOI: 10.1158/1078-0432.CCR-21-0714

personal fees from Pfizer, Merck, AstraZeneca, and SeaGen outside the submitted work. L.A. Carey reports grants from NIH and Bristol Myers Squibb during the conduct of the study. H.S. Rugo reports grants from Pfizer, Merck, Novartis, Lilly, Roche, Odonate, Daiichi, Seattle Genetics, Macrogenics, Sermonix, Boehringer Ingelheim, Polyphor, AstraZeneca, and Immunomedics and personal fees from Puma, Mylan, and Samsung during the conduct of the study. M.C. Liu reports other support from Eisai, Genentech, Merck, Novartis, Seattle Genetics, Tesaro, AstraZeneca, Pfizer, and Genomic Health outside the submitted work. V. Stearns reports grants from Biocept, Pfizer, Novartis, Medimmune, and Puma Biotechnology outside the submitted work and is a member, Data Safety Monitoring Board, Immunomedics, Inc. S. Ramaswamy reports grants from NIH during the conduct of the study. L.W. Ellisen reports grants from NIH, NCI, National Cancer Center, and MGH ECOR and non-financial support from AVON Foundation, BCRF, and Susan G. Komen Foundation during the conduct of the study; in addition, L.W. Ellisen has a patent for RASAL2 biomarker pending. No disclosures were reported by the other authors.

Authors' Contributions

S.-B. Koh: Conceptualization, data curation, formal analysis, funding acquisition, validation, investigation, visualization, methodology, writing–original draft, writing–review and editing. **K. Ross:** Data curation, software, formal analysis, validation, investigation, visualization, methodology, writing–review and editing. **S.J. Isakoff:** Conceptualization, resources, data curation, formal analysis, investigation, writing–review and editing. **N. Melkonjan:** Data curation, validation, investigation, writing–review and editing. **L. He:** Data curation, formal analysis, validation, investigation, writing–review and editing. **K.J. Matissek:** Data curation, formal analysis, validation, investigation, writing–review and editing. **A. Schultz:** Data curation, formal analysis, validation, investigation, writing–review and editing. **E.L. Mayer:** Resources, data curation, writing–review and editing. **T.A. Traina:** Resources, data curation, writing–review and editing. **L.A. Carey:** Resources, data curation, writing–review and editing. **H.S. Rugo:** Resources, data curation, writing–review and editing. **M.C. Liu:** Resources, data curation, writing–review and editing. **V. Stearns:** Resources, data curation, writing–review and editing. **A. Langenbucher:** Data curation, formal analysis, investigation, writing–review and editing. **S.V. Saladi:** Data curation, formal analysis, investigation, writing–review and editing. **S. Ramaswamy:** Resources, writing–review and editing. **M.S. Lawrence:** Resources, writing–review and editing. **L.W. Ellisen:** Conceptualization, resources, formal analysis, supervision, funding acquisition, writing–original draft, writing–review and editing.

Acknowledgments

We thank the Translational Breast Cancer Research Consortium and its three foundation partners (The AVON Foundation, The Breast Cancer Research Foundation, and Susan G. Komen for the Cure), and we are grateful for all the patients and investigators who participated in TBCRC009. Funding was provided by the NCI-AVON Partners for Progress Award 3P30CA06516-45S2 (S.J. Isakoff), and by the Tracey Davis Memorial Fund, Rosanne's Rush for Research, the Boston Chapter of Golfers Against Cancer, and the MGH Executive Committee on Research (ECOR) Research Scholar Award (L.W. Ellisen), and the National Cancer Center, the MGH ECOR Fund for Medical Discovery, and the MGH Cancer Center Excellence Award (S.-B. Koh).

The costs of publication of this article were defrayed in part by the payment of page charges. This article must therefore be hereby marked *advertisement* in accordance with 18 U.S.C. Section 1734 solely to indicate this fact.

Received February 22, 2021; revised April 30, 2021; accepted June 18, 2021; published first June 24, 2021.

References

1. Turner NC, Reis-Filho JS. Tackling the diversity of triple-negative breast cancer. Clin Cancer Res 2013;19:6380–8.
2. Liedtke C, Mazouni C, Hess KR, André F, Tordai A, Mejia JA, et al. Response to neoadjuvant therapy and long-term survival in patients with triple-negative breast cancer. J Clin Oncol 2008;26:1275–81.
3. Tutt A, Tovey H, Cheang MCU, Kernaghan S, Kilburn L, Gazinska P, et al. Carboplatin in BRCA1/2-mutated and triple-negative breast cancer BRCAness subgroups: the TNT Trial. Nat Med 2018;24:628–37.
4. Isakoff SJ, Mayer EL, He L, Traina TA, Carey LA, Krag KJ, et al. TBCRC009: a multicenter phase II clinical trial of platinum monotherapy with biomarker assessment in metastatic triple-negative breast cancer. J Clin Oncol 2015;33:1902–9.
5. Schmid P, Adams S, Rugo HS, Schneeweiss A, Barrios CH, Iwata H, et al. Atezolizumab and nab-paclitaxel in advanced triple-negative breast cancer. N Engl J Med 2018;379:2108–21.
6. Shah SP, Roth A, Goya R, Oloumi A, Ha G, Zhao Y, et al. The clonal and mutational evolution spectrum of primary triple-negative breast cancers. Nature 2012;486:395–9.
7. Hoeflich KP, O'Brien C, Boyd Z, Cavet G, Guerrero S, Jung K, et al. *In vivo* antitumor activity of MEK and phosphatidylinositol 3-kinase inhibitors in basal-like breast cancer models. Clin Cancer Res 2009;15:4649–64.
8. Giltnane JM, Balko JM. Rationale for targeting the Ras/MAPK pathway in triple-negative breast cancer. Discov Med 2014;17:275–83.
9. Ramaswamy B, Mrozek E, Lustberg M, Wesolowski R, Layman R, Abdel-Rasoul M, et al. NCI 9455: phase II study of trametinib followed by trametinib plus AKT inhibitor,GSK2141795 in patients with advanced triple negative breast cancer [abstract]. In: Proceedings of the 107th Annual Meeting of the American Association for Cancer Research; 2016 Apr 16–20; New Orleans, LA. Philadelphia (PA): AACR; Cancer Res 2016;76(14 Suppl):Abstract nr LB-216.
10. Duncan JS, Whittle MC, Nakamura K, Abell AN, Midland AA, Zawistowski JS, et al. Dynamic reprogramming of the kinome in response to targeted MEK inhibition in triple-negative breast cancer. Cell 2012;149:307–21.
11. Zhou B, Zhu W, Jiang X, Ren C. RASAL2 plays inconsistent roles in different cancers. Front Oncol 2019;9:1235.
12. Garnett MJ, Edelman EJ, Heidorn SJ, Greenman CD, Dastur A, Lau KW, et al. Systematic identification of genomic markers of drug sensitivity in cancer cells. Nature 2012;483:570–5.
13. Marchion DC, Cottrill HM, Xiong Y, Chen N, Bicaku E, Fulp WJ, et al. BAD phosphorylation determines ovarian cancer chemosensitivity and patient survival. Clin Cancer Res 2011;17:6356–66.
14. Hennessy BT, Lu Y, Gonzalez-Angulo AM, Carey MS, Myhre S, Ju Z, et al. A technical assessment of the utility of reverse phase protein arrays for the study of the functional proteome in non-microdissected human breast cancers. Clin Proteomics 2010;6:129–51.
15. Campeau E, Ruhl VE, Rodier F, Smith CL, Rahmberg BL, Fuss JO, et al. A versatile viral system for expression and depletion of proteins in mammalian cells. PLoS One 2009;4:e6529.
16. McLaughlin SK, Olsen SN, Dake B, De Raedt T, Lim E, Bronson RT, et al. The RasGAP gene, RASAL2, is a tumor and metastasis suppressor. Cancer Cell 2013;24:365–78.
17. Koh S-B, Courtin A, Boyce RJ, Boyle RG, Richards FM, Jodrell DI. CHK1 inhibition synergizes with gemcitabine initially by destabilizing the DNA replication apparatus. Cancer Res 2015;75:3583–95.
18. Koh S-B, Wallez Y, Dunlop CR, Bernaldo de Quirós Fernández S, Bapiro TE, Richards FM, et al. Mechanistic distinctions between CHK1 and WEE1 inhibition guide the scheduling of triple therapy with gemcitabine. Cancer Res 2018;78:3054–66.
19. Koh S-B, Mascalchi P, Rodriguez E, Lin Y, Jodrell DI, Richards FM, et al. A quantitative FastFUCCI assay defines cell cycle dynamics at a single-cell level. J Cell Sci 2017;130:512–20.
20. Krupke DM, Begley DA, Sundberg JP, Richardson JE, Neuhauser SB, Bult CJ. The mouse tumor biology database: a comprehensive resource for mouse models of human cancer. Cancer Res 2017;77:e67–70.
21. Henderson YC, Chen Y, Frederick MJ, Lai SY, Clayman GL. MEK inhibitor PD0325901 significantly reduces the growth of papillary thyroid carcinoma cells *in vitro* and *in vivo*. Mol Cancer Ther 2010;9:1968–76.
22. Takabatake D, Fujita T, Shien T, Kawasaki K, Taira N, Yoshitomi S, et al. Tumor inhibitory effect of gefitinib (ZD1839, Iressa) and taxane combination therapy in EGFR-overexpressing breast cancer cell lines (MCF7/ADR, MDA-MB-231). Int J Cancer 2007;120:181–8.
23. Warburton C, Dragowska WH, Gelmon K, Chia S, Yan H, Masin D, et al. Treatment of HER-2/neu overexpressing breast cancer xenograft models with trastuzumab (Herceptin) and gefitinib (ZD1839): drug combination effects on tumor growth, HER-2/neu and epidermal growth factor receptor expression, and viable hypoxic cell fraction. Clin Cancer Res 2004;10:2512–24.

24. Wang X, Song H, Yu Q, Liu Q, Wang L, Liu Z, et al. Ad-p53 enhances the sensitivity of triple-negative breast cancer MDA-MB-468 cells to the EGFR inhibitor gefitinib. Oncol Rep 2015;33:526–32.
25. Mallon R, Feldberg LR, Lucas J, Chaudhary I, Dehnhardt C, Santos ED, et al. Antitumor efficacy of PKI-587, a highly potent dual PI3K/mTOR kinase inhibitor. Clin Cancer Res 2011;17:3193–203.
26. Gao J, Aksoy BA, Dogrusoz U, Dresdner G, Gross B, Sumer SO, et al. Integrative analysis of complex cancer genomics and clinical profiles using the cBioPortal. Sci Signal 2013;6:pl1.
27. Cerami E, Gao J, Dogrusoz U, Gross BE, Sumer SO, Aksoy BA, et al. The cBio cancer genomics portal: an open platform for exploring multidimensional cancer genomics data. Cancer Discov 2012;2:401–4.
28. Fekete JT, Győrffy B. ROCplot.org: validating predictive biomarkers of chemotherapy/hormonal therapy/anti-HER2 therapy using transcriptomic data of 3,104 breast cancer patients. Int J Cancer 2019;145:3140–51.
29. Bos PD, Zhang XH-F, Nadal C, Shu W, Gomis RR, Nguyen DX, et al. Genes that mediate breast cancer metastasis to the brain. Nature 2009;459:1005–9.
30. Fan C, Oh DS, Wessels L, Weigelt B, Nuyten DSA, Nobel AB, et al. Concordance among gene-expression-based predictors for breast cancer. N Engl J Med 2006;355:560–9.
31. Perou CM, Sørlie T, Eisen MB, van de Rijn M, Jeffrey SS, Rees CA, et al. Molecular portraits of human breast tumours. Nature 2000;406:747–52.
32. Pitroda SP, Pashtan IM, Logan HL, Budke B, Darga TE, Weichselbaum RR, et al. DNA repair pathway gene expression score correlates with repair proficiency and tumor sensitivity to chemotherapy. Sci Transl Med 2014;6:229ra42.
33. Lehmann BD, Bauer JA, Chen X, Sanders ME, Chakravarthy AB, Shyr Y, et al. Identification of human triple-negative breast cancer subtypes and preclinical models for selection of targeted therapies. J Clin Invest 2011;121:2750–67.
34. Prat A, Parker JS, Karginova O, Fan C, Livasy C, Herschkowitz JI, et al. Phenotypic and molecular characterization of the claudin-low intrinsic subtype of breast cancer. Breast Cancer Res 2010;12:R68.
35. Samatar AA, Poulikakos PI. Targeting RAS-ERK signalling in cancer: promises and challenges. Nat Rev Drug Discov 2014;13:928–42.
36. Turke AB, Song Y, Costa C, Cook R, Arteaga CL, Asara JM, et al. MEK inhibition leads to PI3K/AKT activation by relieving a negative feedback on ERBB receptors. Cancer Res 2012;72:3228–37.
37. Mason JM, Morrison DJ, Basson MA, Licht JD. Sprouty proteins: multifaceted negative-feedback regulators of receptor tyrosine kinase signaling. Trends Cell Biol 2006;16:45–54.
38. Lito P, Pratilas CA, Joseph EW, Tadi M, Halilovic E, Zubrowski M, et al. Relief of profound feedback inhibition of mitogenic signaling by RAF inhibitors attenuates their activity in BRAFV600E melanomas. Cancer Cell 2012;22:668–82.
39. Chen C-H, Hsia T-C, Yeh M-H, Chen T-W, Chen Y-J, Chen J-T, et al. MEK inhibitors induce Akt activation and drug resistance by suppressing negative feedback ERK-mediated HER2 phosphorylation at Thr701. Mol Oncol 2017;11:1273–87.
40. Carey LA, Rugo HS, Marcom PK, Mayer EL, Esteva FJ, Ma CX, et al. TBCRC 001: randomized phase II study of cetuximab in combination with carboplatin in stage IV triple-negative breast cancer. J Clin Oncol 2012;30:2615–23.
41. Ghandi M, Huang FW, Jané-Valbuena J, Kryukov GV, Lo CC, McDonald ER, et al. Next-generation characterization of the Cancer Cell Line Encyclopedia. Nature 2019;569:503–8.
42. Curtis C, Shah SP, Chin S-F, Turashvili G, Rueda OM, Dunning MJ, et al. The genomic and transcriptomic architecture of 2,000 breast tumours reveals novel subgroups. Nature 2012;486:346–52.
43. Pereira B, Chin S-F, Rueda OM, Vollan H-KM, Provenzano E, Bardwell HA, et al. The somatic mutation profiles of 2,433 breast cancers refines their genomic and transcriptomic landscapes. Nat Commun 2016;7:11479.
44. Feng M, Bao Y, Li Z, Li J, Gong M, Lam S, et al. RASAL2 activates RAC1 to promote triple-negative breast cancer progression. J Clin Invest 2014;124:5291–304.
45. Hall CA, Wang R, Miao J, Oliva E, Shen X, Wheeler T, et al. Hippo pathway effector Yap is an ovarian cancer oncogene. Cancer Res 2010;70:8517–25.
46. Zanconato F, Cordenonsi M, Piccolo S. YAP/TAZ at the roots of cancer. Cancer Cell 2016;29:783–803.
47. Chang S-S, Yamaguchi H, Xia W, Lim S-O, Khotskaya Y, Wu Y, et al. Aurora A kinase activates YAP signaling in triple-negative breast cancer. Oncogene 2017;36:1265–75.
48. Nguyen CDK, Yi C. YAP/TAZ signaling and resistance to cancer therapy. Trends Cancer 2019;5:283–96.
49. Zanconato F, Forcato M, Battilana G, Azzolin L, Quaranta E, Bodega B, et al. Genome-wide association between YAP/TAZ/TEAD and AP-1 at enhancers drives oncogenic growth. Nat Cell Biol 2015;17:1218–27.
50. Zhang H, Liu C-Y, Zha Z-Y, Zhao B, Yao J, Zhao S, et al. TEAD transcription factors mediate the function of TAZ in cell growth and epithelial-mesenchymal transition. J Biol Chem 2009;284:13355–62.
51. Kim MH, Kim J. Role of YAP/TAZ transcriptional regulators in resistance to anti-cancer therapies. Cell Mol Life Sci 2017;74:1457–74.
52. Wang X, Qian C, Yang Y, Liu M-Y, Ke Y, Qian Z-M. Phosphorylated Rasal2 facilitates breast cancer progression. EBioMedicine 2019;50:144–55.
53. Moore AR, Rosenberg SC, McCormick F, Malek S. RAS-targeted therapies: is the undruggable drugged? Nat Rev Drug Discov 2020;19:533–52.
54. He Q, Jing H, Liaw L, Gower L, Vary C, Hua S, et al. Suppression of Spry1 inhibits triple-negative breast cancer malignancy by decreasing EGF/EGFR mediated mesenchymal phenotype. Sci Rep 2016;6:23216.
55. Coussy F, El Botty R, Lavigne M, Gu C, Fuhrmann L, Briaux A, et al. Combination of PI3K and MEK inhibitors yields durable remission in PDX models of PIK3CA-mutated metaplastic breast cancers. J Hematol Oncol 2020;13:13.
56. Maiello MR, D'Alessio A, Bevilacqua S, Gallo M, Normanno N, De Luca A. EGFR and MEK blockade in triple negative breast cancer cells. J Cell Biochem 2015;116:2778–85.
57. Boasberg PD, Redfern CH, Daniels GA, Bodkin D, Garrett CR, Ricart AD. Pilot study of PD-0325901 in previously treated patients with advanced melanoma, breast cancer, and colon cancer. Cancer Chemother Pharmacol 2011;68:547–52.
58. LoRusso PM, Krishnamurthi SS, Rinehart JJ, Nabell LM, Malburg L, Chapman PB, et al. Phase I pharmacokinetic and pharmacodynamic study of the oral MAPK/ERK kinase inhibitor PD-0325901 in patients with advanced cancers. Clin Cancer Res 2010;16:1924–37.
59. Haura EB, Ricart AD, Larson TG, Stella PJ, Bazhenova L, Miller VA, et al. A phase II study of PD-0325901, an oral MEK inhibitor, in previously treated patients with advanced non-small cell lung cancer. Clin Cancer Res 2010;16:2450–7.
60. Harada C, Kawaguchi T, Ogata-Suetsugu S, Yamada M, Hamada N, Maeyama T, et al. EGFR tyrosine kinase inhibition worsens acute lung injury in mice with repairing airway epithelium. Am J Respir Crit Care Med 2011;183:743–51.
61. Costa DB, Nguyen K-SH, Cho BC, Sequist LV, Jackman DM, Riely GJ, et al. Effects of erlotinib in EGFR mutated non-small cell lung cancers with resistance to gefitinib. Clin Cancer Res 2008;14:7060–7.

Published OnlineFirst June 24, 2021; DOI: 10.1158/1078-0432.CCR-21-0714

Clinical Cancer Research

RASAL2 Confers Collateral MEK/EGFR Dependency in Chemoresistant Triple-Negative Breast Cancer

Siang-Boon Koh, Kenneth Ross, Steven J. Isakoff, et al.

Clin Cancer Res 2021;27:4883-4897. Published OnlineFirst June 24, 2021.